Journal of Earth and Atmospheric Research

EXPLORATION OF MARBLE DEPOSITS USING REMOTE SENSING AND ELECTRICAL RESISTIVITY METHODS IN OGALE, NORTHCENTRAL NIGERIA

Ademeso, O.A[1]., Akinlalu, A.A[2]., Ajigo, I.O.[1], Ogundele, R.A.[1] and Afolabi, D.O[2].

[1]Department of Applied Geology, Federal University of Technology, Akure, Nigeria
[2]Department of Applied Geophysics, Federal University of Technology, Akure, Nigeria

Article History
Received: 02-05-24
Accepted: 30-05-24

Keywords:
Marble mineralization, Ogale, Igarra Schsit belt, Geoelectric Sounding, ASTER

ABSTRACT

The Igarra Schist belt is known for its vast carbonate mineralization potential, chief among them being Marble deposits. However, there has been little exploration work to map the extent of the marble deposits in the regions of the Igarra schist belt. Hence, this study integrated remote sensing (advanced spaceborne thermal emission reflection radiometer (ASTER) and geoelectric sounding datasets for the reliable mapping and delineation of marble deposits in the Ogale area. RGB band combinations and decorrelation stretch on bands (3, 9, 14), (4, 9, 8), (4, 6, 8), (14, 8, 6), (14, 8, 4), (8, 4, 3), (6, 8, 9) and (4, 8, 9) were applied to map marble mineralization in the study area. The results of these analyses showed the western part of the study area showed the most potential of marble mineralization. Patches were also observed at the southern and eastern parts of the study area. In addition, six geoelectric sounding data were obtained in areas delineated as having marble mineralization potential from ASTER analyses. The geoelectric results showed that the study area is underlain by three to five geologic/geoelectric units comprising the top soil, lateritic layer, clay, weathered basement and the marble hosted basement. The marble deposits are observed to have relatively moderate resistivity as a result of being hosted within the schist rocks in the study area. Furthermore, eight correlation panels of the columnar sections produced for the geoelectric sounding results showed that marble mineralization has an apparent dip towards the western part of the study area which explains the extensive potential in that part of the study area from ASTER analyses. The depth to the marble deposit across the study area was also observed to occur at an average depth of 10 m, indicating that marble mineralization in the study area is occurring at shallow depth. The study concluded that concludes that ASTER and geoelectric sounding datasets are effective in the mapping of marble deposits.

Correspondence: aaakinlalu@futa.edu.ng

1 INTRODUCTION

The construction industry has experienced rapid growth due to increasing population growth, urbanization and industrialization in Nigeria with Cements being one of the important materials used in driving the construction industry. This has also led to increasing demand in limestone and marble, two raw materials used interchangeably

in the manufacture of cement (RMRDC, 2001; Fatoye and Gideon, 2013). Despite both rocks (limestone and marble) having similar chemical and mineralogical characteristics, marble is preferred in the production of cement and other building and construction purposes. This is because of the reduced porosity of marble, making it to be more durable than limestone. In addition, because marble occurs in more diverse colors than limestone, it has become a sought after raw material in building and construction purposes because of its aesthetic appeal (Abatan *et al.,* 1993; FMIC, 1999).

Due to these apparent advantages of marble over limestone, the demand of marble in the construction industry has skyrocketed in recent years. This has also put a strain on mining companies to vigorously exploit marble deposits in different locations in Nigeria in order to meet the increasing demand of marble deposits (Onimisi *et al.,* 2015).

Marble deposits in Nigeria are enormous and found in different parts of the country, cutting across Cross River, Edo, Kogi, Kwara, Nasarawa and Oyo States including the Federal Capital Territory (F.C.T) (KPMG, 2017). Marble deposits in these locations are well documented in various research texts (Fatoye and Gideon, 2013; Onimisi *et al.,* 2015; Ozegin, 2019; Ajigo *et al.,* 2020). Marble deposit occurrences in Ogale area of Kogi State, the study area, have been reported to occur within the metasedimentary and granite rocks. They are essentially carbonate rocks being a product of the metamorphism of limestone. The association of Marble deposits with iron ore mineralization in several parts of the Northcentral of Nigeria, including the study area has increased the exploration and exploitation efforts of Marble (Obaje, 2009). However, despite several documented texts on the occurrences and exploration of marble deposits in various locations in Kogi State and its environs, no research has been done in the study area with focus on the extent of marble mineralization and subsurface characterization.

Geological mapping often involve random sampling and surface mapping which cannot give a holistic view of the extent of mineralization and information on subsurface characterization (Akinlalu *et al.,* 2024). The use of remote sensing imageries and airborne geophysical methods on the other hand has been found adequate in exploration program for the precise and detailed mapping of marble deposits especially for large area extent (Odeyemi *et al.,* 1997a).

Remote sensing imageries like Atmospheric Spaceborne Thermal Emission Reflection Radiometer (ASTER), Landsat and Sentinel datasets have been used by several researchers in the mapping of marble deposits due to the distinct spectral characteristics of different alteration minerals and absorbed minerals related to marble mineralization. Hence, by mapping clay minerals, ferric iron absorptions and calcium carbonate minerals which are genetically related to marble mineralization, marble deposits can be adequately mapped using remote sensing imageries. Detailed information can be found in the texts of Gaffey (1986); Clark (1999).

Also, the use of geophysical methods especially electrical resistivity and electromagnetic methods has also been found to be relevant methods in the

exploration of marble deposits in different geological settings of the world. This is hinged on their ability to distinguish marble deposit occurrences from the country rocks due to the distinct resistivity and conductivity contrast that exist between marble deposits and country rocks. Furthermore, they are important methods in determining the depth extent and lateral extent of marble deposit (Aina and Olorunfemi, 1996; Odeyemi *et al.,* 1997a; Onimisi *et al.,* 2015; Ozegin *et al.,* 2019).

The thrust of this work therefore involved a detailed follow up investigation of marble exploration from geological mapping by employing remote sensing imageries and electrical resistivity in the delineation of marble deposits in Ogale area of Kogi State.

2. Geological Setting and Mineralization

The study area, Ogale, Kogi State, Northcentral Nigeria falls within the Precambrian Basement complex. It is part of the Igarra Schist belt which extends from Edo to Kogi State. It is characteristically made up of majorly metasediments and metavolcanics which dominate the study area (Odeyemi 1988, 1990). Rock units in the area consist of Migmatites, biotite, including low–grade metasediments consisting of Schists, Marbles, Calc–Silicates, and Quartzites. There are further evidences of intrusions of granitoids into the Schists and Gneisses which are principally trending in the approximate E–W direction, indicating a strong imprint of the Kibaran orogeny in the study area. The geological assemblages in the study area suggest a long period of sedimentation and different episodes of intense tectonism (Odeyemi *et al.,* 1997b). Common feature of the Igarra Schist belt is the presence of calcareous rocks and conglomerates in different parts of the belt, and Gneisses at the margins of the belt (Obaje, 2009).

Odeyemi (1993) revealed that the main structural unit of the belt is the NW trending open synform assimilated into the earlier formed E–W folds during the Kibaran orogeny. The different orientations of the geological and structural units in the belt and association with the Pan–African granitoids gave further evidences of the Kibaran orogeny in the study area (Obaje, 2009).

Like most Schist belt in the world, the Igarra schist belt is known for its mineralization potential especially in relation to the occurrence of calcareous mineral deposits like limestone and marble due to the basal environment it is found, often marked by a general presence of carbonates. The study area is majorly underlain by lithologic units such as Charnockite, Granite Gneiss, Calc – Gneiss/Marble, Quartz Schist, Biotite Schist and Migmatite/Gneiss (Figure 1).

The marble deposit in the study area is found within the migmatite-gneiss-schist-quartzite complex as imprints of sedimentary carbonate rocks (Obaje, 2009; Olade, 2019). It is a product of metamorphism of limestone.

Evidences of marble mineralization are marked by CO_3^{2-} alteration haloes along geologic contacts and faults in different geologic units in the study area such as metasediments and the Gneisses (Olade, 2019).

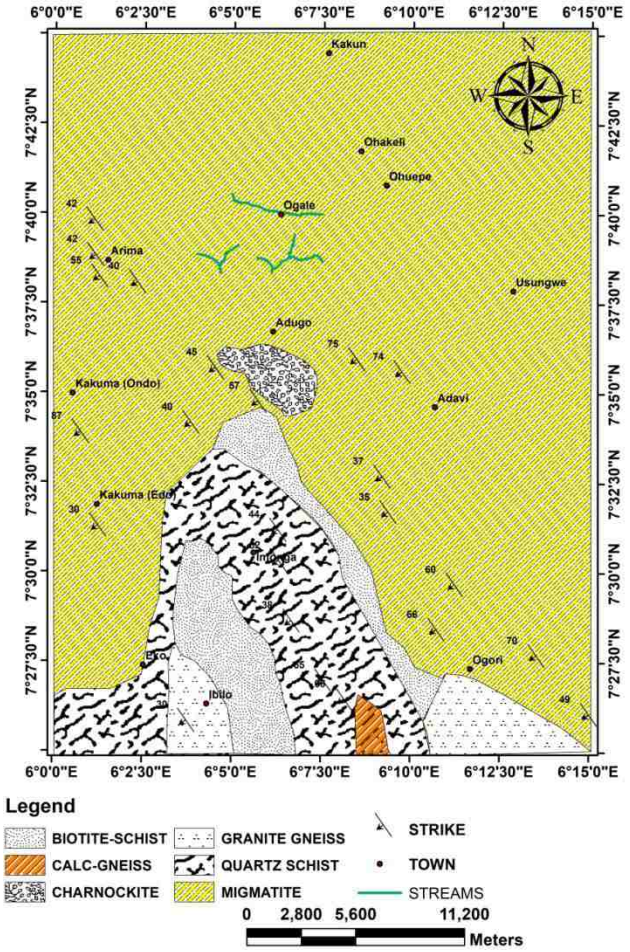


Figure 1: Geological Map of the Study Area (Modified after Ajigo *et al.,* 2020)

1. Materials and Methodology

Two datasets involving the advanced spaceborne thermal emission reflection radiometer (ASTER) and geoelectric resistivity sounding were utilized for prospecting for marble deposit in the study area.

Remote Sensing (ASTER) Dataset

The ASTER imagery acquired on the TERRA platform for ASTER sensor usually travels in a near circular, sun-synchronous orbit with an inclination of approximately 98.2°, an altitude of 705 km and a repeat cycle of 16 days. ASTER sensor offers relatively improved spatial, spectral, and temporal resolutions for the identification of mineral and rocks, provided there exists a significant absorption contrast with the neighbouring rocks (Rajendran *et al*., 2011a, b, 2012; Rajendran and Nasir, 2013a, b; Madani, 2014). ASTER sensor measures visible reflected radiation in three spectral bands (visible near infra-red (VNIR) between 0.52 and 0.86 μm with 15 m spatial resolution) and infrared reflected radiation in six spectral bands (short wavelength infra-red (SWIR) between 1.6 and 2.43 μm with 30 m spatial resolution). ASTER sensor records the data in band 3B (0.76–0.86 μm) with a backward-looking angle that enables the calculation of Digital Elevation Model (DEM) (Table 1).

For the present study, the ASTER imagery was downloaded on 23rd September, 2023 from the archive of the United States Geological Survey (USGS) (https://earthexplorer.usgs.gov/). The data was received in Tag Image File Format which provides files for each band containing the ASTER imagery and an ASCII text.met file containing the metadata. The ASTER data was supplied in terms of scaled radiance at-sensor data with radiometric and geometric corrections applied by Earth and Remote Sensing Data Analysis Center (ERSDAC) Japan. The imagery was checked for sensor errors (such as banding and other geometric distortions) and found in

Table 1: Sensor characteristics of ASTER Instruments (After Andogma *et al.,* 2021)

Sensor Characteristics	ASTER VNIR	SWIR	TIR
Spectral bands with range (μm)	Band 01 0.52-0.60 (Nadir looking)	Band 04 1.6-1.7	Band 10 8.125-8.475
	Band 02 0.63-0.69 (Nadir looking)	Band 05 2.145-2.185	Band 11 8.475-8.825
	Band 03N 0.76-0.86 (Nadir looking)	Band 06 2.185-2.225	Band 12 8.925-9.275
	Band 03B 0.76-0.86 (Backward looking)	Band 07 2.235-2.285	Band 13 10.25-10.95
		Band 08 2.295-2.365	Band 14 10.95-11.65
		Band 09 2.36-2.43	
Spatial resolution (nm)	15	30	90
Swath width (km)	60	60	60
Radiometric resolution (bits)	8	8	12
Cross track pointing	±318 km (±24°)	±116 km (±8.55°)	±116 km (±8.55°)

cloud cover of 0%. Thereafter, the images were georeferenced in the 32N Universal Transverse Mercator (UTM) projection and World Geodetic System of 1984 (WGS-84) ellipsoid datum. The fourteen VNIR–SWIR–TIR spectral bands acquired for the Ogale area were resized to the site of interest using ENVI (5.3), SNAP, and ArcGIS (10.3) software.

The pre–processing of ASTER imagery involved crosstalk correction to correct for energy leak from one band to another (Iwasaki and Tonooka, 2005). In this study, Cross-Talk correction software available from www.gds.aster.ersdac.or.jp was used to remove this effect of energy leaking. Subsequently, the spectral bands of ASTER were layer stacked to compose the multispectral images into a single image with the same spatial and target resolutions. The Terra ASTER L1T dataset (8 bits signal quantization levels, solar azimuth 166^0, solar elevation 37^0) was calibrated to radiance data in IDL ENVI version 5.4.1 by applying appropriate gain and offset values. The spectral bands of ASTER were layer stacked to compose the multispectral images into a single image with the same spatial and target resolutions. Atmospheric correction was also applied by Fast Line-of-sight Atmospheric Analysis of Spectral Hypercubes (FLAASH) algorithm on VNIR and

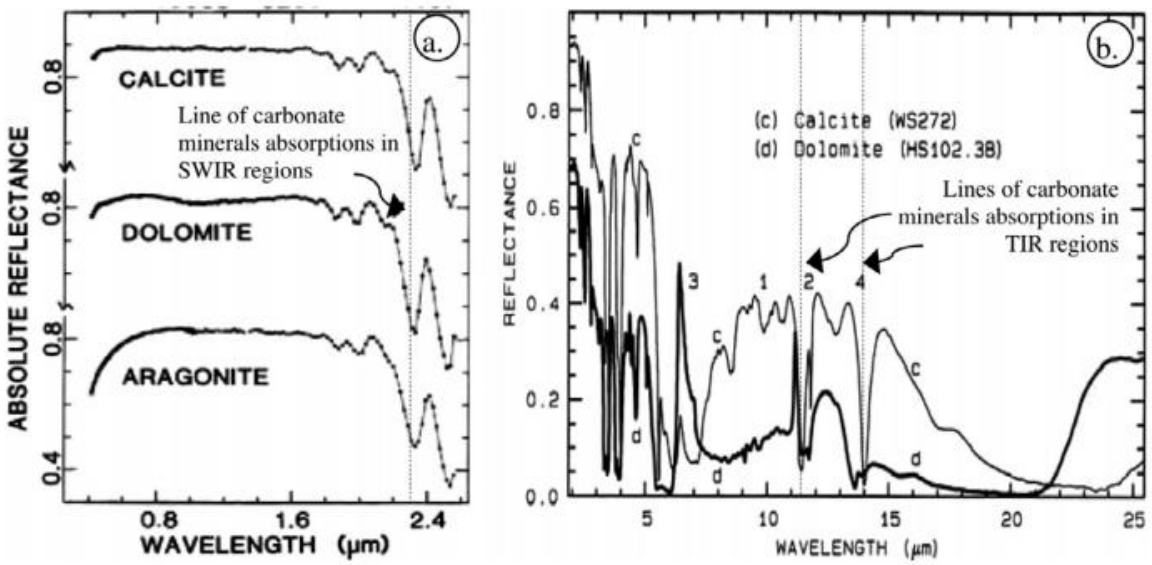


Figure 2: The Spectral Absorptions of (a) Calcite, Dolomite, and Aragonite in the SWIR Regions (Gaffey, 1986) and (b) Calcite and Dolomite in TIR Region (Clark, 1999

SWIR of ASTER subsystems (Thome *et al.,* 1998) by considering parameters such as atmospheric model, aerosol model, aerosol retrieval, platform used, synoptic time, scene coordinates, and acquisition date of the acquired ASTER data. In addition, a log residual algorithm was applied to the VNIR+SWIR+TIR (visible and near–infrared+shortwave infrared+thermal infrared) subsystems of ASTER data.

To properly delineate marble mineralization in the study area, the spectral library plots of major carbonate minerals stacked from the USGS Spectral Library for minerals (Envi 5.3) were employed to choose the most appropriate spectral bands for marble mapping in the area (Figure 2). The ASTER image spectra of major carbonate rocks of the regions in ASTER VNIR–SWIR (ASTER band 1 to band 9) and ASTER TIR (ASTER band 10 to band 14) were constrained with the spectra plots in Figures 2a and b for de-masking marble formation in the area.

The carbonate rocks and fossils (such as lime mud, glauconites, oncolites, corals, monotonous species of bioclasts, foraminifera, ostracods, molluscs, ammonite and carbonaceous detritus) present in the study area are mainly composed of calcium carbonates (CO_3^{2-}). Since ASTER sensor has a diagnostic CO_3^{2-} absorption features near 2.31–2.33 μm wavelengths in the ASTER spectral band 8 (SWIR region) and 11.2 μm wavelengths in band 14 (TIR region) (Table 1; Figure 2), the pre-processed ASTER data was used to map marble deposit.

Band 6 was used to map clay minerals due to its Al–OH absorption characteristics near 2.20 μm wavelength. The ferric (Fe^{+3}) and ferrous (Fe^{+2}) irons absorptions that occur around 0.45 μm wavelength in ASTER band 1 and 1.0–1.1 μm wavelengths in ASTER band 3 were used to discriminate iron rich weathered surface. Also, the Si–O absorption near 8.7 μm wavelength in band

11 was used to map quartz alteration since it enables the identification of quartz and silicate minerals (Rowan *et al.,* 1986; Ninomiya *et al.,* 2005; Mars and Rowan, 2006; Baldridge Baldridge *et al.,* 2009; Mars and Rowan, 2011; Rajendran *et al.,* 2011a).

Based on the spectral absorption characters of carbonate minerals, the marble formation was discriminated from the adjoining schist using image processing methods such as Red-Green-Blue (RGB) colour composition and decorrelation stretching (DS). RGB composition of spectral bands such as bands 14, 8, 4; bands 4, 6, 9; bands 4, 6, 8 were used to highlight marble deposits in the study area. In the case of False Colour Composite (FCC), the spectral bands 4, 6, and 8 of ASTER data and spectral bands of 3, 6, and 9 were displayed through three colour channels, namely red (R), green (G), and blue (B). These three additive colours were used to display multispectral bands in a colour composite, where the spectral response of the carbonate mineral indicates peaks of reflectance ratio.

Decorrelation stretch was likewise used to remove the high correlation that is common with multispectral data sets. Decorrelation stretch technique was used to produce a more colourful colour composite image that improves the visualization of ASTER images for marble identification (Gillespie *et al.,* 1986).

Geoelectric Resistivity Sounding Data

Geoelectric data were acquired using the Ohmega Resistivity meter and its accessories. The geoelectric survey involved the Vertical Electrical Sounding (VES) using the Schlumberger array. A total of six (6) points were occupied in the study area. The electrode spacing was varied between 1–100 m. The resistivity data were presented as field curves (by plotting the apparent resistivity (ρa) against AB/2 or half the spread of the electrode spacing on a bi–logarithm paper). The data were interpreted qualitatively by visual inspection of the field curves and further interpreted quantitatively by partial curve matching (Koefoed, 1979) with the help of master curves (Orellana and Mooney, 1966) and auxiliary charts (Zohdy, 1965; Keller and Frischnecht, 1966) to obtain initial estimates of resistivity and thickness of the various geoelectric layers at each VES location. These geoelectric parameters were used as starting models for forward modelling using the WinResist™ software (Vander Velpen, 2004). The software received the manually derived parameters as inputs for a starting geoelectric model and iteratively improved on it until the error is minimized to an acceptable level. From the interpretation of the resistivity data, values for layers resistivity and thickness were derived. The results of the interpretation of the resistivity data presented as curve types and columnar sections assisted in delineating the Marble and schist. The depth to top of marble is also delineated. The method also assisted in having idea about the lateral extent of occurrence of the Marble deposit in the study area. Furthermore, the results obtained also assisted in characterizing the subsurface layers obtainable in the area. It is important to note that marble deposit especially in Schist hosted environment like the study area are indicated by relatively high resistivity values. Hence, areas of relatively high resistivity values from the geoelectric parameters could be indicative of Marble deposits.

Results and Discussion

ASTER Dataset

RGB Composite Maps

The RGB colour blending of ASTER spectral bands in the region of SWIR-TIR wavelengths was used to de-mask marble and dolomite deposits from the adjoining metasedimentary rocks, due to their emissivity and absorption characteristics. The ASTER spectral 14 in TIR region at the absorption position of 11.2 µm served as diagnostics for carbonate minerals occurring with the marbles and dolomites in the study area.

Due to the peculiarity of marble and dolomite deposits in Ogale area of Igarra Schist belt, which are not exclusively calcium carbonates but contain other minerals like quartz, the combination of ASTER 3 and 9 spectral bands was used to highlight the surficial expressions of alumino-silicate and carbonate minerals that are occurring with the investigated area. The observed low emissivity signature of ASTER 14 band (TIR spectral region), which is depicted in yellow colouration, is suspected to be due to the presence of marbles and dolomites in the study area (Figure 3). The strong absorption of incident electromagnetic energy in ASTER VNIR-SWIR-TIR wavelength regions in the study area is typical of the presence of carbonate minerals in the Ogale area, Igarra Schist belt. Also, the observed strong dark absorption signatures in the entire ASTER SWIR-TIR wavelength regions in the area are most likely due to the poor absorption of electromagnetic energy in the visible near infrared, shortwave infrared and energy emission in the thermal infrared wavelengths in and around water bodies of the study area (Figure 3). On the other hand, the dark tone of red colour observed across the study area is presumably due to the presence of carbonaceous marbles and dolomites that occur in and around streams of water (Figure 3).

The observed light red colouration region overprinting green colouration, that is localized at the northern and eastern flanks of the study area, is presumably due to the presence of carbonate and silicate minerals that is occurring with the migmatite, and calc-silicate gneiss rocks (Figure 3).

The underlying green colouration on Figure 3 served as an indicator for silica content in some lithologies such as Migmatite, and Calc-silicate Gneiss rocks in the area. ASTER sensitivity characteristics of schist (yellow colouration due to low reflectance of spectral band 14) are well-expressed in the study area.

In the same vein, the presence and spatial distribution of marble and dolomite occurring with schist in the study area can be diagnostically highlighted on the Red-Green-Blue (RGB) colour composition map (Figure 4) by considering the spectral sensitivities of the calcium carbonate (CO_3^{2-}) minerals on ASTER spectral bands 4 (1.60–1.70 µm), 9 (2.36–2.43 µm), 8 (2.295–2.365 µm). Among the three bands, wavelength of band 4 resonates to the occurrence of alumina silicate minerals that are occurring with Migmatite, and Calc-silicate Gneiss in the study area. Band 8 is sensitive to the presence of carbonate and hydroxyl bearing minerals of Marble and Dolomite deposits. Band 9 assisted to reinforce the absorption property of carbonate

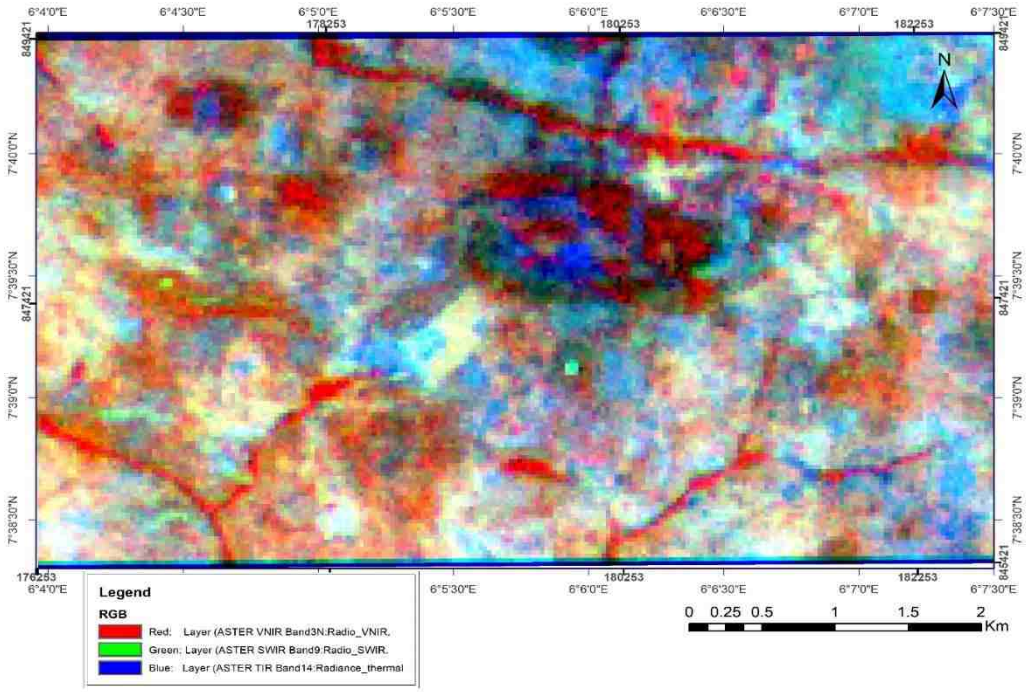


Figure 3: Red-Green-Blue Composition of ASTER bands 3, 9, and 14 of the Study Area

minerals at their vibration position (2.33–2.45 μm). The strong absorption and high reflectance features on ASTER SWIR bands 8 and 9, due to the presence of CO_3^{2-} and O-H in the marble and dolomite deposits, could be responsible for the dark-reddish tone observed across the study area (Figure 4).

The observed reddish colouration, especially at the north-western and eastern parts of the study area, is presumably due to the surficial manifestation of carbonate minerals present in the marble deposits (Figure 4). The observed green colouration with high reflectance on the ASTER SWIR 4, 9, 8 bands are well pronounced across the study area. These observed greenish zonations are most likely due to the occurrence of hydroxyl bearing alumina-silicate and carbonates minerals in the encountered lithologies. Likewise, a prominent red colouration is observed at the north-western part of the study area (Figure 4). These zones with high emissivity are indicative of hydroxyl bearing alumina-silicate minerals, most especially on schist rocks.

Furthermore, in an attempt to demarcate marble and dolomites from the schist, based on the surficial reflectance of electromagnetic energy in the study area, the sensitivities of ASTER bands 4, 6, 8 in the SWIR wavelength region were presented as RGB colour composite (Figure 5). The absorption of band 8 at positions 2.295–2.365 μm was used to serve as a pointer to the presence of carbonate minerals occurring with the sought marble and dolomite deposits. The strong absorption and high reflectance features on ASTER SWIR band 8, due to the presence of CO_3^{2-} and O-H, are displayed as sky blue across the study area (Figure 5). The ASTER SWIR spectral bands of 4 and 6 were also used to highlight the

presence of schist and laterites in the study area due to Al–OH absorption that occurred near 2.20 µm wavelength. It was observed that the well-exposed and dominant metasedimentary lithologies in the study area are Migmatite and Calc-silicate Gneiss, which are evident by the overprinting of red colouration in the area (Figure 5).

Although the mineralized zones are not well-exposed as the other metasedimentary rocks in the study area, it is possible that Marbles and Dolomites might be occurring at depths beneath schist and Granite Gneiss lithologies in the area. The yellow imprints that are observed across the study area stemmed from the absorption of bands 6 and 8, which could be as a result of the presence of silicates and carbonates minerals that are contained in Marble and Dolomite deposits (Figure 5). The resonance of vibration at wavelength 1.60 – 1.70 µm (ASTER band 4) over silicates present in some encountered lithologies of migmatite (e.g. schist, granites, and quartzites) is responsible for the overprinting red colouration, especially in the southern part of the study area (Figure 5).

Figure 6 shows the RGB composite map of bands 14, 8 and 6 in an attempt to demarcate marble mineralization from the neighbouring rocks, especially Schist and granites. The presence of CO_3^{2-} in marble and dolomites was highlighted from the absorption features of ASTER 14 and 8 spectral bands (Figure 6). Also, the ASTER SWIR spectral band of 6 was used to highlight schist bodies in the study area (Figure 6). The presence of surficial expression of schists is well accentuated on RGB of 14, 8 and 6 with a characteristic blue colouration. The high emissivity from the interaction of electromagnetic incident energy with the hydroxyl bearing

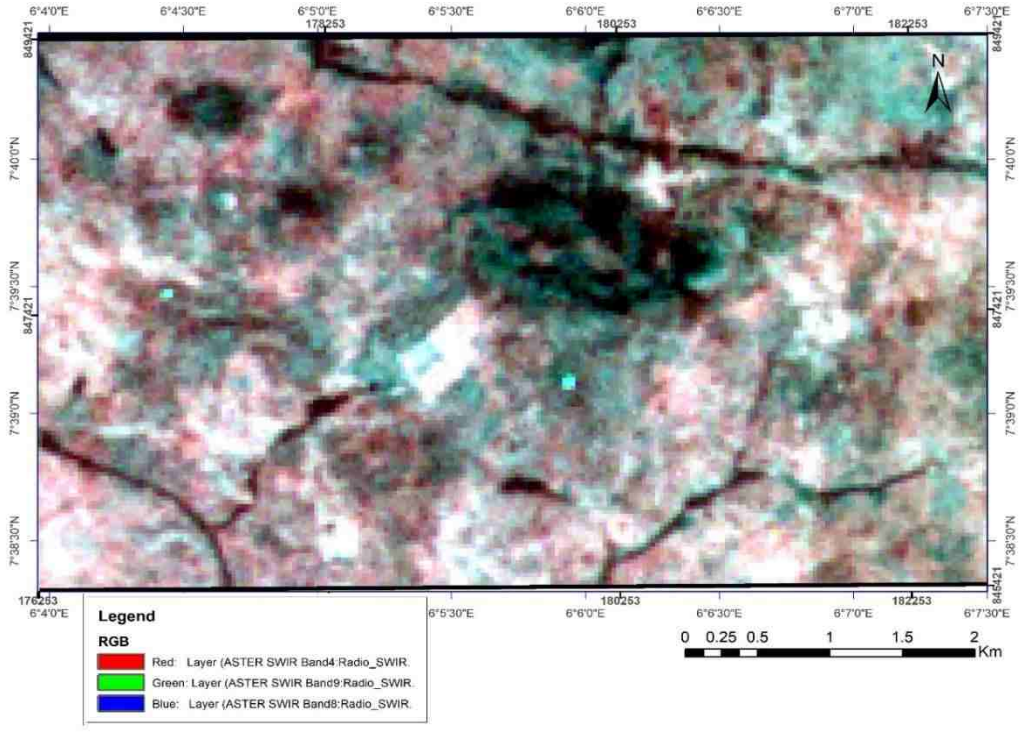


Figure 4: Red-Green-Blue Composition of ASTER bands 4, 9, and 8 of the Study Area

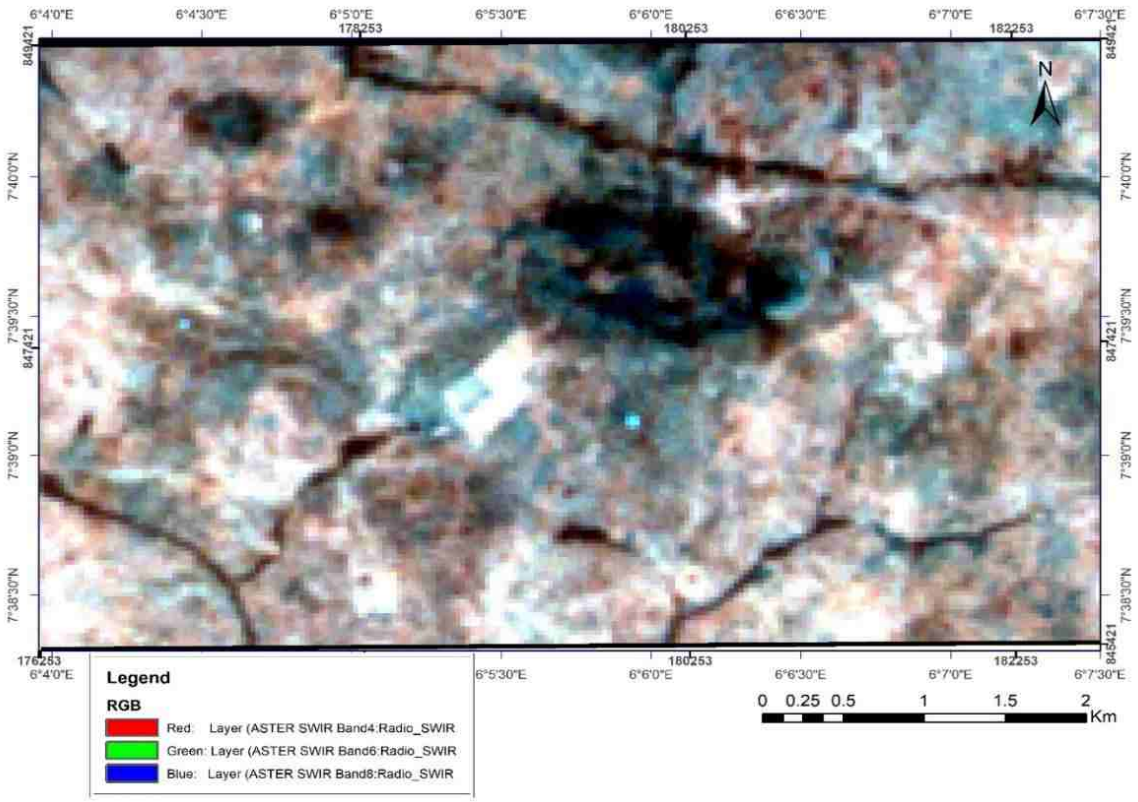


Figure 5: Red-Green-Blue Composition of ASTER bands 4, 6, and 8 of the Study Area.

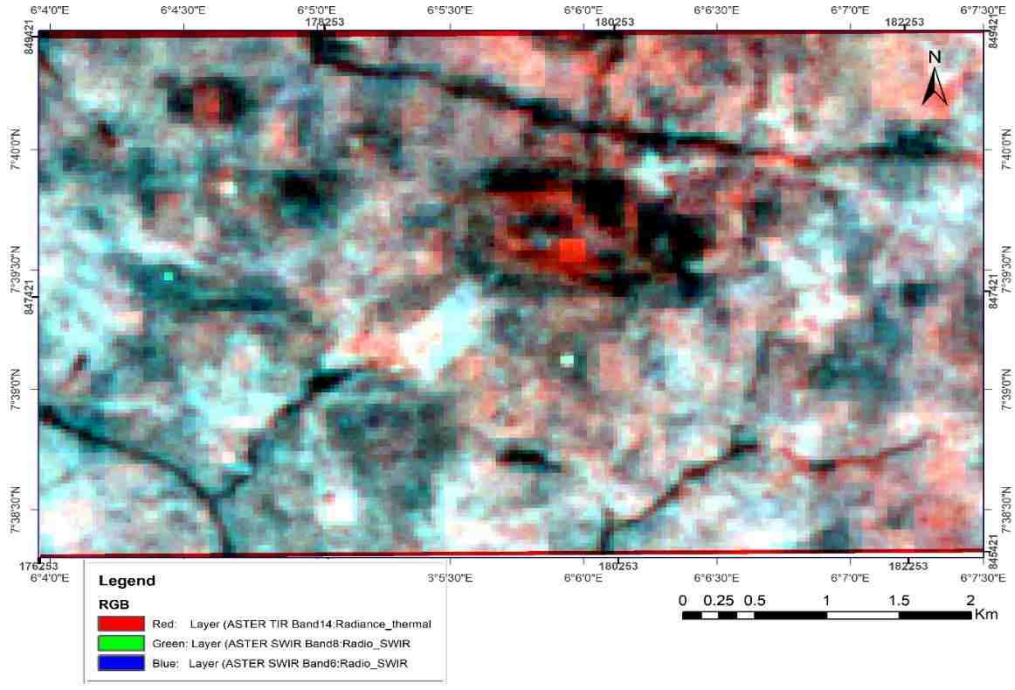


Figure 6: Red-Green-Blue Composition of ASTER bands 14, 8, and 6 of the Study Area.

alumina-silicate minerals present in schists could be responsible for the blue colouration in the northern part of the study area (Figure 6). The prominent green colouration at the southern part of the study area, which are signatures of strong absorption from 14 and 8 spectral bands, are possibly due to the presence of carbonate minerals in the marbles and dolomites where schist serves as the host (Figure 6).

In addition, the striking cyan colouration that is observed at the northwestern and eastern parts of the study area is typical of twinning calcium carbonates and silicates minerals in marbles and dolomites. The observed strong dark absorption signatures in the entire ASTER SWIR-TIR wavelength regions in the area are most likely due to the poor absorption of electromagnetic energy in the visible near infrared, shortwave infrared and energy emission in the thermal infrared wavelengths in and around water bodies of the study area (Figure 6).

Figure 7 shows the RGB composite map of the study area for bands 14, 8 and 4 in the region of SWIR–TIR wavelengths. This was done to essentially de-mask marble and dolomite deposits from the adjoining lithologies based on the emissivity and absorption characteristics of spectral bands adopted in this study. The ASTER spectral band 14 in TIR absorption position of 11.2 μm was used to delineate calcium carbonate minerals occurring with marble and dolomite in the hosting schist bodies of the study area. Due to the silicification on marble and dolomite deposits of Ogale area, Igarra Schist belt, which are not exclusively calcium carbonates but also contain silicate minerals, the combination of ASTER 4 and 8 spectral bands was used to highlight the surficial expressions of alumina silicate and carbonate minerals that are occurring with the marble deposits.

The strong absorption of incident electromagnetic energy in ASTER VNIR-SWIR-TIR wavelength regions in the study area are characterised by the presence of carbonate minerals in the study area (Figure 7). The observed blue colouration with hues of yellow patches that is apparent across the study area is an indication of strong absorption of ASTER spectral band 4 at the wavelength position between 1.60 – 1.70 μm, which is characteristic of carbonate minerals present in marble and dolomite deposits in the study area (Figure 7). However, the marble-rich zones within the study area are well-accentuated by the overwhelming light green colouration that is observed at the western and eastern parts of the study area. These potential mineralised zones are much related to the absorption threshold of carbonate minerals on ASTER spectral band 8. The presumable marble deposits in the area intruded the hosting schist rock, and plunge approximately NE-SW.

Likewise, dark blue colouration that is observed at the northwestern part of the study area may be connected to the grade of metamorphism and tectonic deformation on silicate-rich schist and schistose lithologies.

In the same vein, RGB colour composite maps of bands 8, 4 and 3 was used to damask marble and dolomite mineralized zones in the study area. The resonance of vibration at the absorption position of band 8 (2.33–2.45 μm) was used to further accentuate the presence of the carbonaceous and

siliceous marble and dolomite deposits in the study area (Figure 8). Band 4 was used because it usually resonates to the presence of alumina silicate minerals at positional wavelengths of 1.60 – 1.70 µm. Band 3 was used to characterize the general albedo of the geologic materials, especially the iron-rich weathered surface like laterites.

The strong absorption and high reflectance features on ASTER SWIR band 8, due to the presence of CO_3^{2-} and Mg-O-H, are displayed as brownish yellow colouration in the northwestern and eastern parts of the study area (Figure 8). These suspected marble-rich zones in the area could be related to the overprinting of spectral band 8 on spectral band 4 because of the twinning carbonate and silicate minerals.

The green colouration across the study area could be characteristic of absorption and emissivity of spectral reflectance in band 4, which is much related to the presence of Al-O-H in schist and granites rocks in the area. The subtle yellow patches that are observed with the green colouration (background spectral signatures), succinctly expressed at the northern part of the study area, are likely connected to the presence of CO_3^{2-} contained in the marble and dolomite deposits of Ogale area, Igarra Schist belt (Figure 8).

Figure 9 shows the RGB composite map of the study area by utilizing ASTER spectral bands 6, 8 and 9. This was done to reinforce the absorption vibration due to the presence of calcium carbonates (2.31 – 2.34 µm) in dolomites and marble. Due to the H-O-H compositional features in schists, laterites and granites, spectral band 6 was used to delimit these lithologies from the marble deposits in the area.

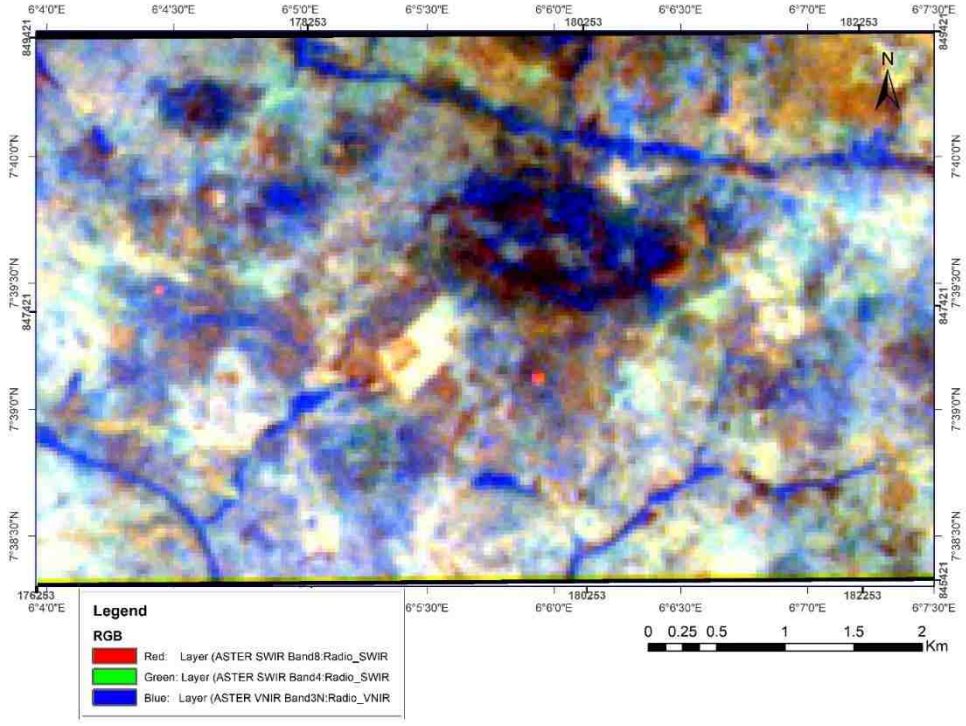


Figure 8: Red-Green-Blue Composition of ASTER bands 8, 4 and 3 of the Study Area

The spectral characteristic of Fe, Mg-OH group, which is common to schists, was displayed on ASTER spectral band 6 as pink colouration (Figure 9). This pinkish colouration, which is related to the occurrence of schists and laterites, is vividly seen at the northern and central parts of the study area. The overwhelming blue colouration that is prominent at the southern part of the study area is typical of silicate bending and stretching modes present in granites and schists (Figure 9).

However, the presence of carbonate minerals in marble and dolomite deposits is much related to the green colouration across the study area especially in the south of the investigated area (Figure 9).

In addition, RGB composite colour map of bands 4, 8 and 9 was used to further highlight the locales that are impregnated with marble and dolomite deposits. ASTER SWIR-VNIR spectral bands of 4 and 8 were colour blended to accentuate the occurrence of marble and dolomite deposits due to their carbonate's composition. Most especially, band 4 usually vibrates at absorption wavelength of 1.60–1.70 μm in the presence of carbonates contained in marble and dolomite deposits, and it is shown as orange colouration in the southern part of the study area (Figure 10).

The green colouration that is observed at the northwestern and eastern parts of the study area, due to the absorption features of band 8, is much related to the presence of carbonates in marble but with higher grade metamorphism (Figure 10). There are some blue streaks that are observed across the study area, they are much connected to the presence of weathered schists and granites. The apparent dark absorption features observed in the study area are typical of poor absorption of

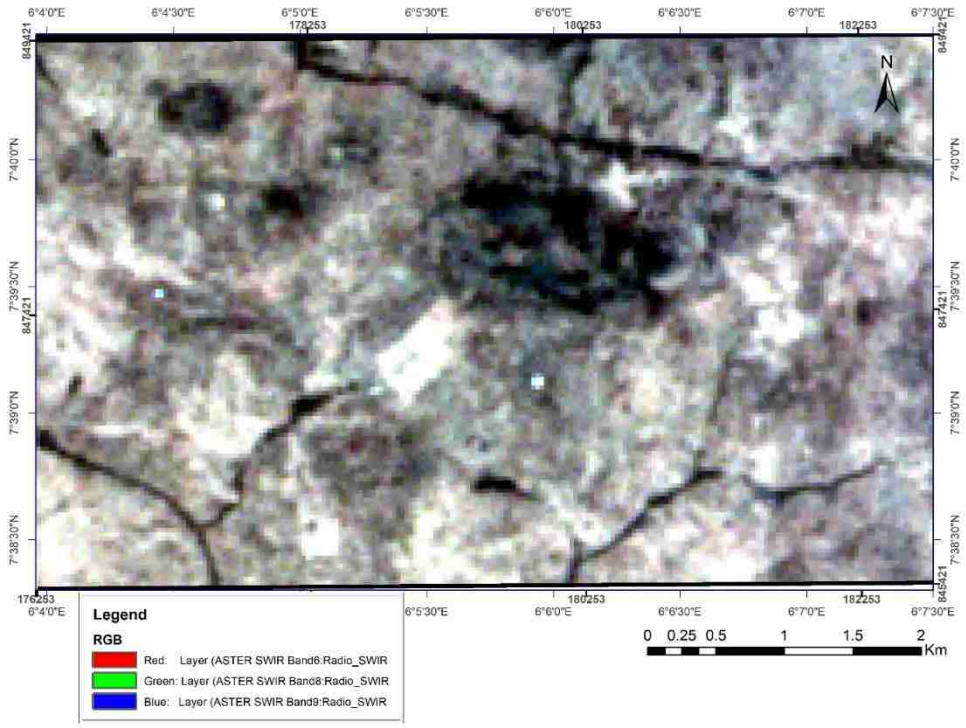


Figure 9: Red-Green-Blue Composition of ASTER bands 6, 8 and 9 of the Study Area.

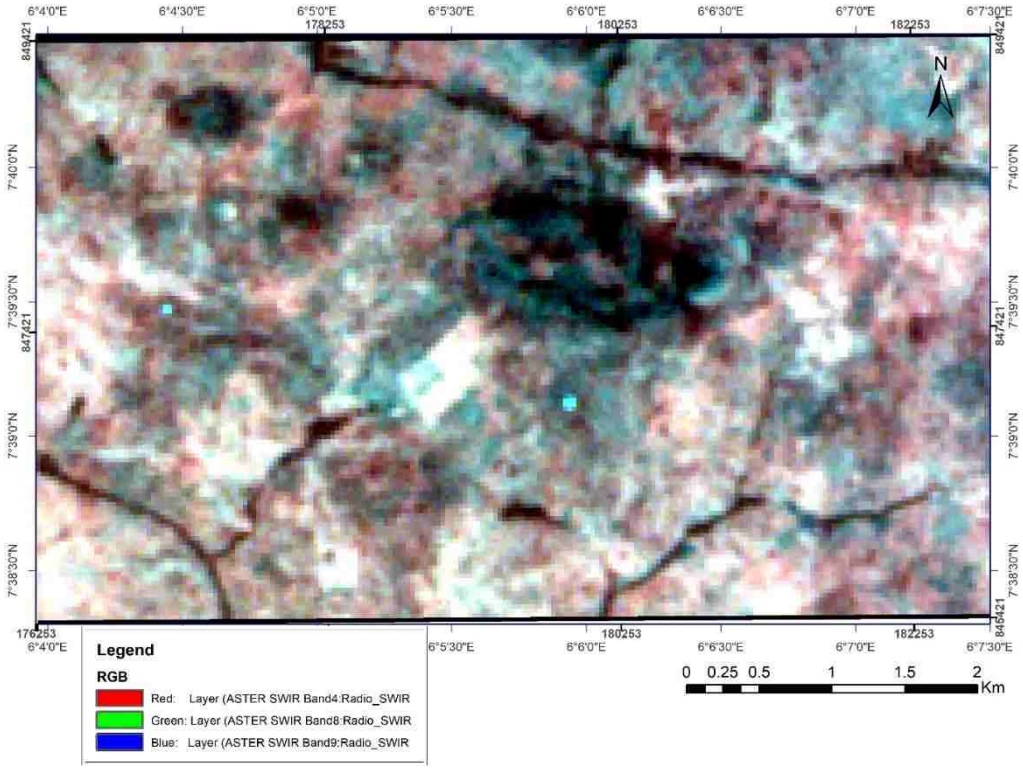


Figure 10: Red-Green-Blue Composition of ASTER bands 4, 8 and 9 of the Study Area.

electromagnetic energy in and around water bodies of the study area due to poor reflectance surface of water bodies present in the area (Figure 10).

Decorrelation Stretch of ASTER Imagery

The occurrences and spatial distribution of marble and dolomite deposits were mapped by decorrelation stretch (digital image processing) method using the spectral sensitivities of carbonate minerals in the study area on ASTER spectral bands 8 (2.295–2.365 μm), 3 (0.78–0.86 μm), and 1(0.52–0.60 μm) (Figure 11). Among the three bands, band 8 responds to the presence of carbonate and hydroxyl bearing minerals of the marble and dolomite deposits. Band 3 was used to characterize the general albedo of the geologic materials, especially the iron-rich weathered surface like laterites. Meanwhile, band 1 contains information relating to the presence of iron minerals that are associated with the laterites overlying the study area. The blue patches that are widespread across the study area are typical of the ferric (Fe^{+3}) and ferrous (Fe^{+2}) irons absorptions around 0.45 μm wavelength. Hence, the absorbed ferric and ferrous irons at ASTER band 1 could be primarily due to the presence of leached laterites at the surface. The green colouration that is vividly seen across the study area is an indication of the occurrence of silicate bending and stretching modes that are occurring with laterites, schists and granites (Figure 11).

The observed strong absorption features of ASTER band 8, which are the reflection of the presence of carbonate in the marble deposits, are seen across the study area as purple colouration. Also, the prominent yellow colouration that is

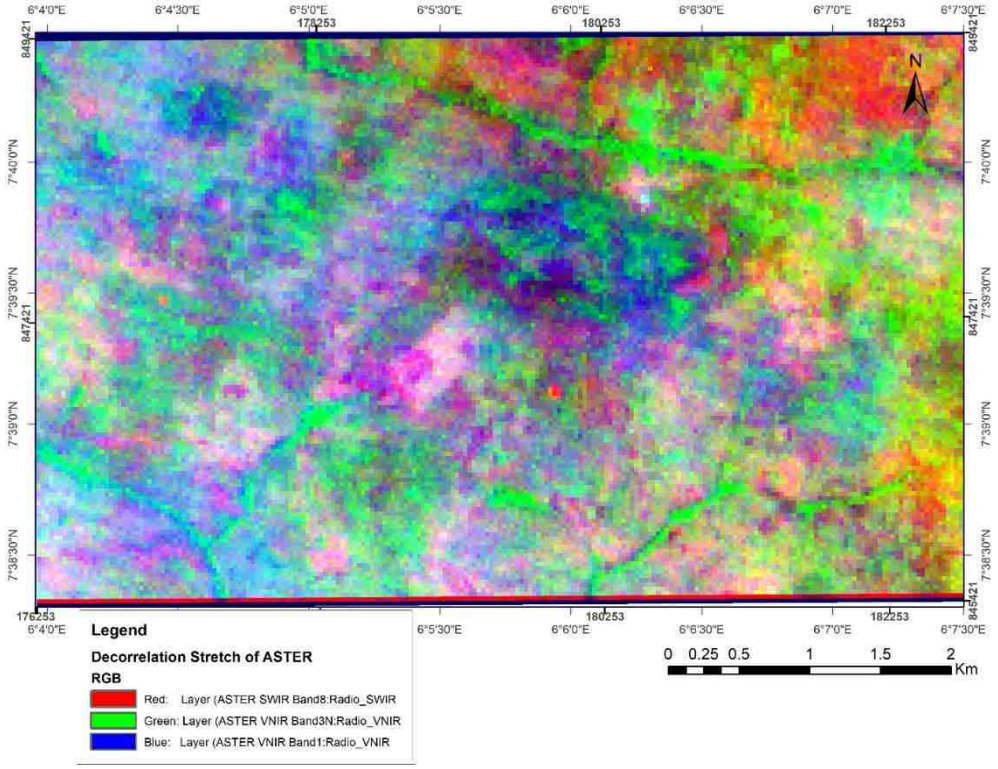


Figure 11: Decorrelation Stretch Colour Composite of ASTER bands 8, 3, and 1 of the Study Area

observed at the northeastern and eastern parts of the study area is an indication of carbonate and quartz rich minerals present in these locales. Based on the spectral characteristics (i.e. yellow colouration) at these suspected mineralized zones, it is most likely that the marble and dolomite deposits are overlain with weathered laterites and schists in the study area (Figure 11).

Figure 12 shows the decorrelation stretch of ASTER bands 8, 4 and 3. Band 8 was used to highlight the presence of carbonate minerals in marble and dolomite deposits due to the vibration process of CO_3^{2-}. Due to Al–O–H and Si–O–H present in some rocks in the study area, ASTER band 3 was used to highlight the presence of iron-rich weathered surface like laterites in the area. As a result of silicification on marble and dolomite of Igarra Schist belt, band 4 was used to detect the presence of alumina silicate bending minerals occurring with the mineral deposits. The pinkish strong absorption suspected over the mineralised zones could stemmed from the vibration and absorption processes of ASTER bands 4 and 8 in the study area. The presence of schists is subtly defined as green colour across the study area. Although, the presence of marble is expressed on the decorrelated map as light green colouration, the diagnostic colour blends of ASTER bands 8, 4, and 3 are random and chaotic (Figure 12).

Furthermore, due to the vibrational processes in the lattice environments both in radical and molecules of Al–OH and Mg–OH present in clays, micas, amphiboles and schists, decorrelation stretch was performed on bands 4, 9 and 8. The green colouration observed at the northwestern and western part of the study area indicates the

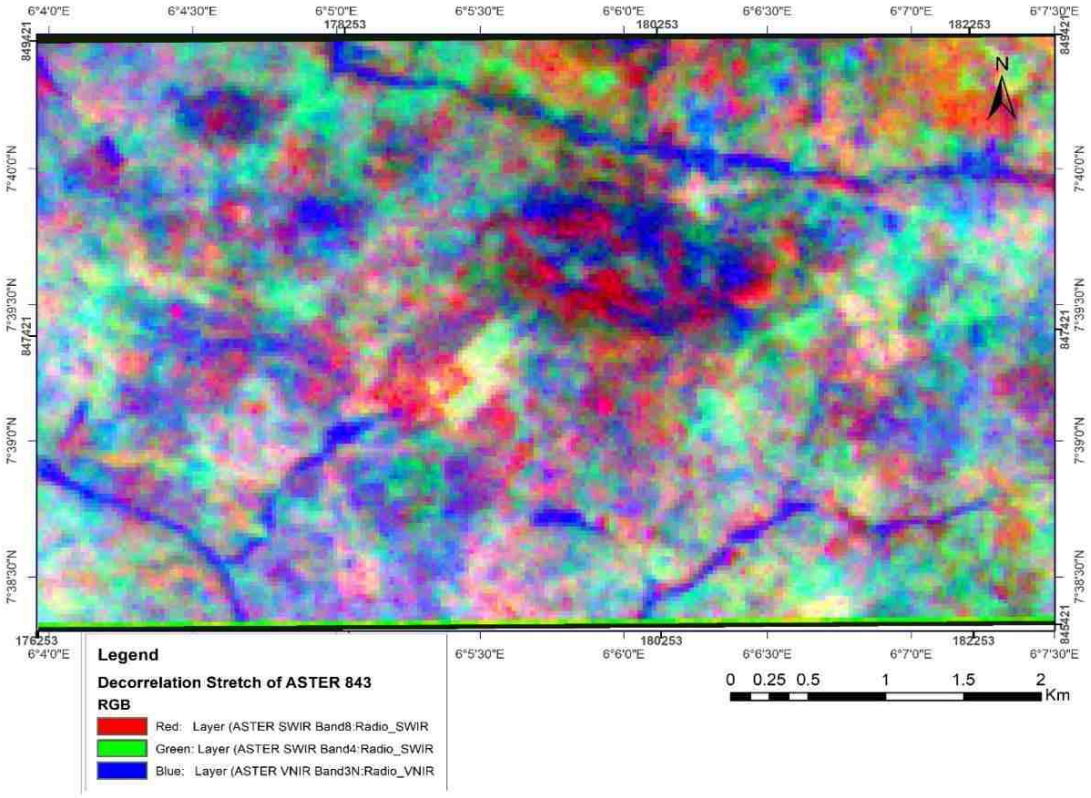


Figure 12: Decorrelation Stretch Colour Composite of ASTER bands 8, 4, and 3 of the Study Area.

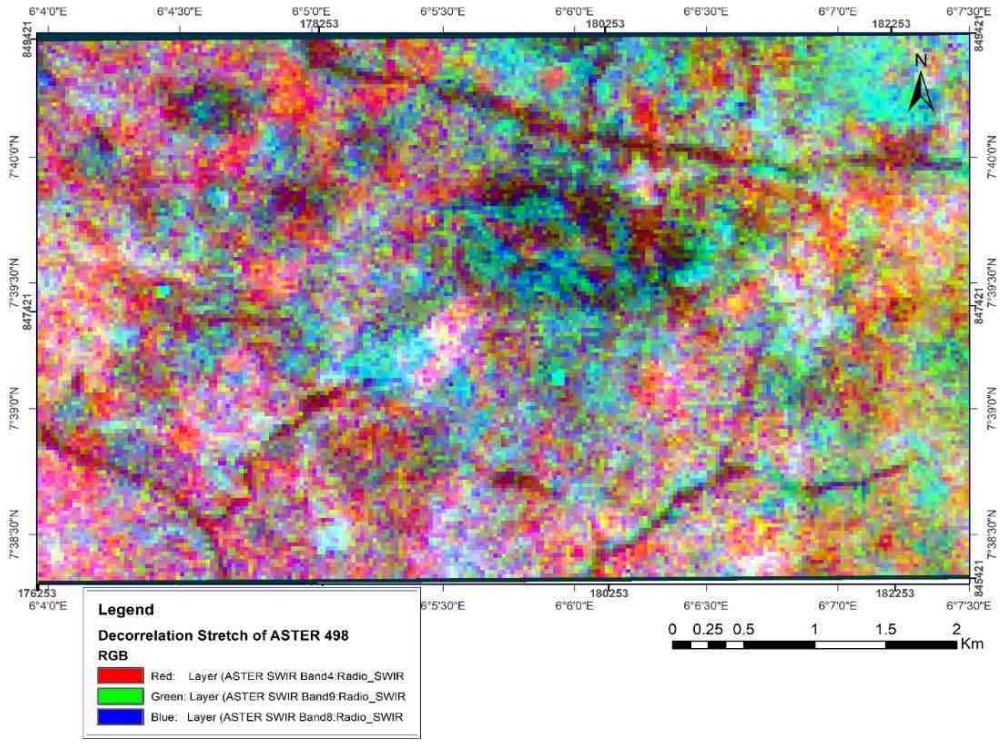


Figure 13: Decorrelation Stretch Colour Composite of ASTER bands 4, 9 and 8 of the Study Area.

presence of schists and laterites (Figure 13). The dark strong absorption features occurring with country rock (i.e. schists) in the area are the indications of poor reflectance water surfaces from the incident electromagnetic energy spectrum. Band 4 was used to detect the presence of alumina silicate bending minerals occurring with the mineral deposits, and it is displayed as red colouration (Figure 13).

Carbonate minerals such as calcite ($CaCO_3$), and dolomite [$CaMg(CO_3)_2$] show significant useful narrow absorption features around 2.35 μm, corresponding to band 8 (2.295–2.365 μm) due to C–O bonds in their compositions. Since, marble and dolomite rocks occur mainly with minerals rich in CO_3, Al-OH, Mg-OH and H_2O contents which have unique spectral absorptions characters, the presence of marble and dolomite mineral deposits in the area are shown as cyan colour. This is due to the presence of carbonate and silicate minerals at these locales (Figure 13).

Prospect Map of Marble Mineralization

Figure 14 shows the marble mineralisation potential map of the study area produced from the integration of the RGB and decorrelation stretch colour composite maps of various ASTER bands. The map shows that marble can be found in the western and southeastern part and a small portion in the northern section of the study area. The map further shows that the western part of the study area has more

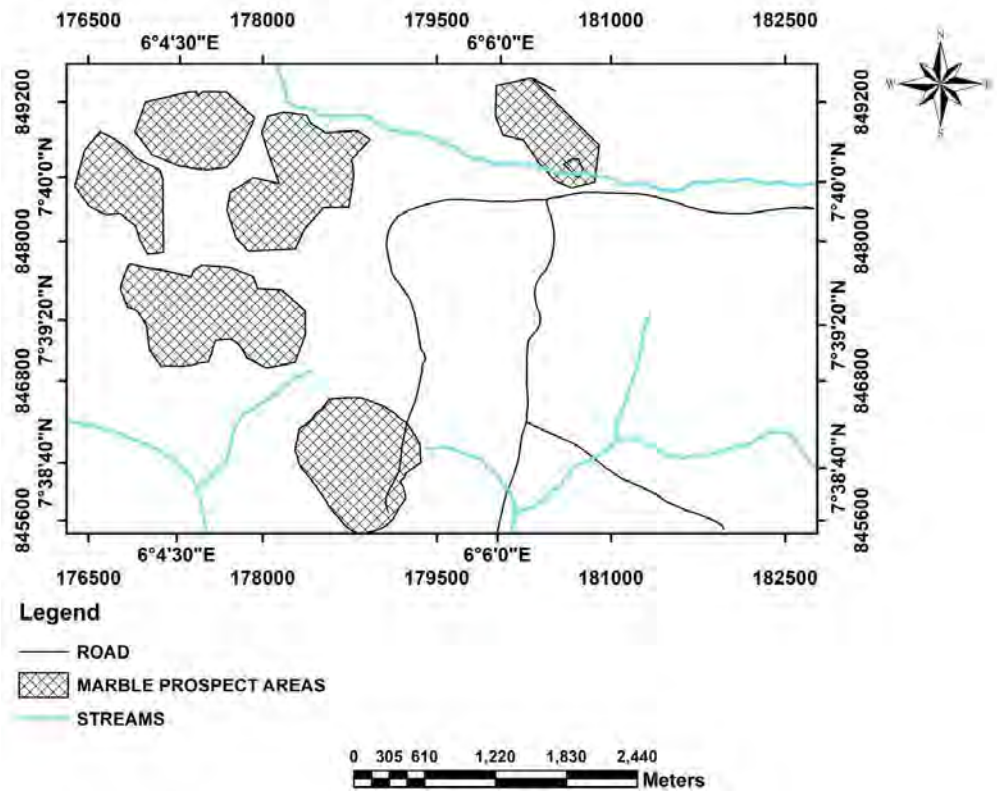


Figure 14: Marble Prospectivity Map of the Study Area Obtained from the Analysis of the ASTER Data

potential of marble mineralization.

Geoelectric Sounding Data

The choice of the points for the resistivity sounding was informed by the location of outcropping marble deposits in the study area and zones of probable marble locations delineated from the remote sensing analyses. Two (2) VES points, VES 1 and VES 2 were used as control VES locations as they are located around outcropping marble deposits. VES 4 and VES 6 are located within Marble prospective zones in the southern and northwestern parts of the study area respectively (Figure 15). On the other hand, VES 3 is located at the rim of another Marble prospective zone in the northern part of the study area due to the difficulty encountered on the field in accessing the prospective zone. VES 5 is not located around any delineated prospective zone due to the accessibility of the prospective zones, hence, the point was chosen based on prevailing geological condition and to have an even distribution of the VES points in the investigated area.

In addition, the columnar sections for the VES locations were correlated with each other to characterize the subsurface and determine the lateral extent of the marble deposit in the investigated area. Hence, fifteen correlation panels were established for this study.

Sounding Curves

The curve types obtained from the geoelectric field data in the investigated area are KHA for

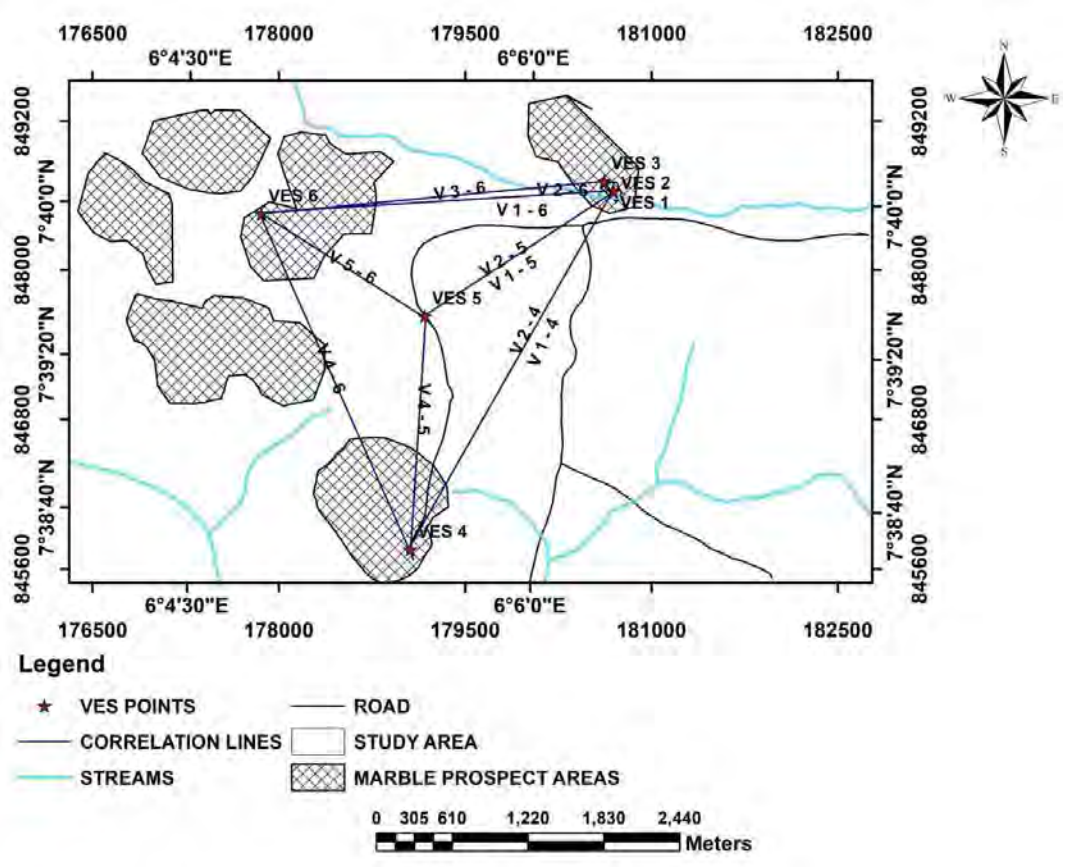


Figure 15: Marble Prospectivity Map of the Study Area showing the VES Points and Correlation Lines

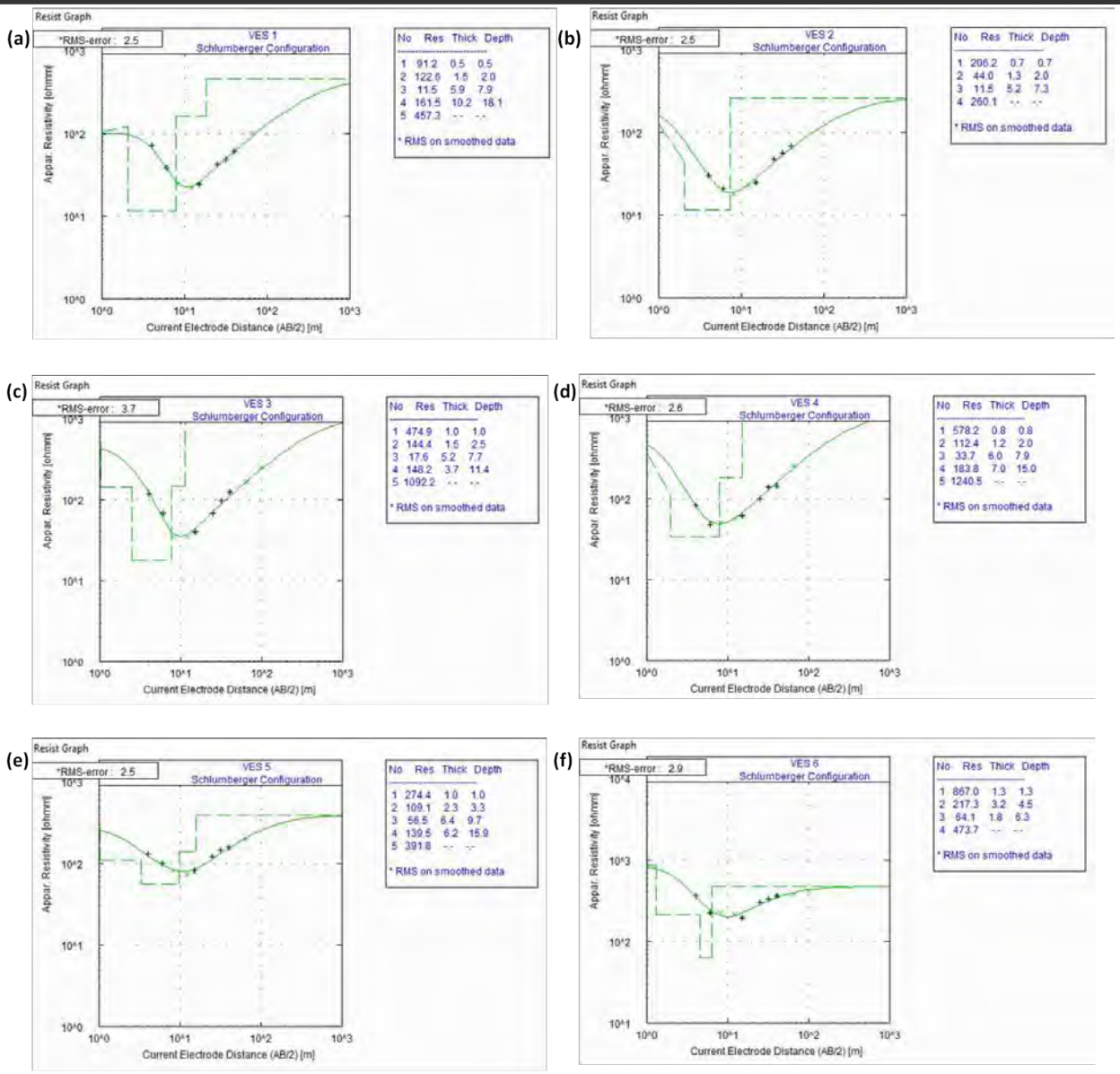


Figure 16: Sounding Curves obtained for (a) VES 1 (b) VES 2 (c) VES 3 (d) VES 4 (e) VES 5 and (f) VES 6

VES 1; QH for VES 2 and VES 6; QHA for VES 3, VES 4 and VES 5. Quantitative interpretation of the sounding curves revealed that the area is underlain by Top Soil, Lateritic Clay, Weathered Basement and the Fresh basement Schist hosted Marble. The resistivity values of the study area range from 12–1241 Ωm with thickness values in the range of 0.5 m to 18.1 m for the layers above the bedrock, and indeterminate for the underlying bedrock.

Figure 16 (a–f) shows the sounding curves obtained in the study area.

Correlation Panel of the Columnar Sections

Figure 17 shows the correlation panel connecting columnar sections of VES 1 and VES 4.

The columnar sections obtained for VES 1 and VES 4 identified four geoelectric/geologic subsurface layers which include the top soil, suspected marble deposit, Clay and fresh

basement with relatively high resistivity value. The top soil has resistivity values in the range of 91–578 Ωm with thickness values in the range of 0.5–0.8 m. This layer is underlain by suspected marble deposit with resistivity values in the range of 112–123 Ωm and thickness values in the range of 1.2–1.5 m; Clay with resistivity values in the range of 12–34 Ωm with thickness values in the range of 5.9–6 m. This is underlain by another layer of suspected marble deposit with resistivity values in the range of 162–184 Ωm and thickness values in the range of 7–10.2 m. The last layer with resistivity values in the range of 457–1241 Ωm with infinite thickness is the fresh basement (Figure 17).

The distance between VES 1 and VES 4 is 3,318 m. The underlying geoelectric/geologic layers for both columnar sections correlate well with each other, howbeit with varying thicknesses especially for the suspected marble deposit. The depth to the top of the Marble at VES 4 is observed to be deeper than VES 1, with an observable dip towards the southwestern part of the study area at VES 4. The lateral extent of the Marble deposit is approximately 3,318 m based on the distance between the two VES points (Figure 17).

Figure 18 shows the correlation panel connecting columnar sections of VES 1 and VES 6.

The columnar sections obtained for VES 1 and VES 6 identified four geoelectric/geologic subsurface layers which include the top soil, suspected marble deposit, Clay and fresh basement with relatively high resistivity value. The top soil has resistivity values in the range of 91–867 Ωm with thickness values in the range of

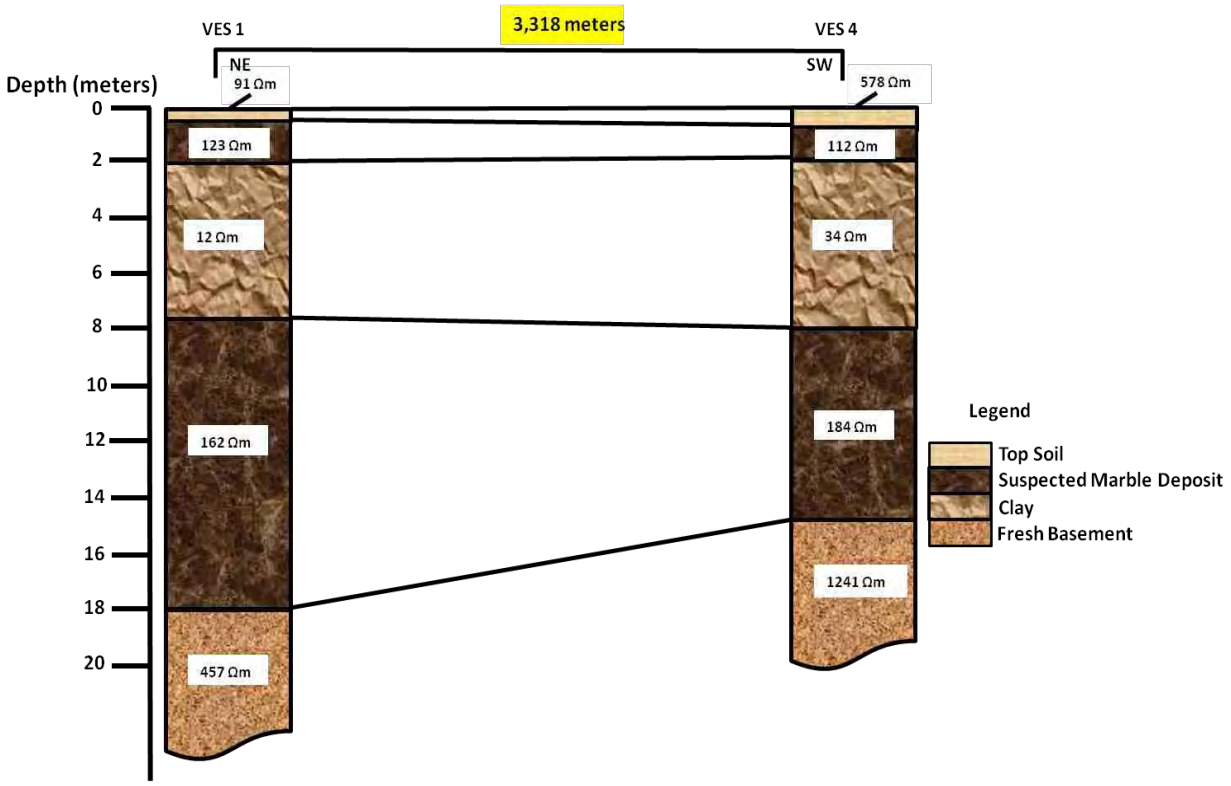


Figure 17: Correlation Panel for Columnar Sections for VES 1 and VES 4

0.5–1.3 m. This layer is underlain by suspected marble deposit with resistivity values in the range of 123–217 Ωm and thickness values in the range of 1.5–4.5 m; Clay with resistivity values in the range of 12–64 Ωm and thickness values in the range of 3.2–5.9 m. There is another suspected marble deposit with resistivity value of 162 Ωm and thickness value of 10.2 m at VES 1. The last layer with resistivity values in the range of 457–474 Ωm with infinite thickness is the fresh basement (Figure 18).

The distance between VES 1 and VES 6 is 2,858 m. The underlying geoelectric/geologic layers for both columnar sections correlate well with each other, howbeit with varying thicknesses especially for the Top soil, suspected marble deposit and Clay. The depth to the top of the Marble at VES 6 is observed to be shallower than VES 1, with an observable dip towards the northwestern part of the study area at VES 1. Furthermore, the suspected marble deposit is observed to be truncated by clay layer and continuous at a depth of about 7.6 m on VES 1. However, this layer is observed to be absent at VES 6. The lateral extent of the Marble deposit is approximately 2,858 m based on the distance between the two VES points (Figure 18).

Figure 19 shows the correlation panel connecting columnar sections of VES 2 and VES 5. The columnar sections obtained for VES 2 and VES 5 identified three to four geoelectric/geologic subsurface layers which include the top soil, Lateritic Clay, suspected marble deposit, Clay and fresh basement with relatively high resistivity

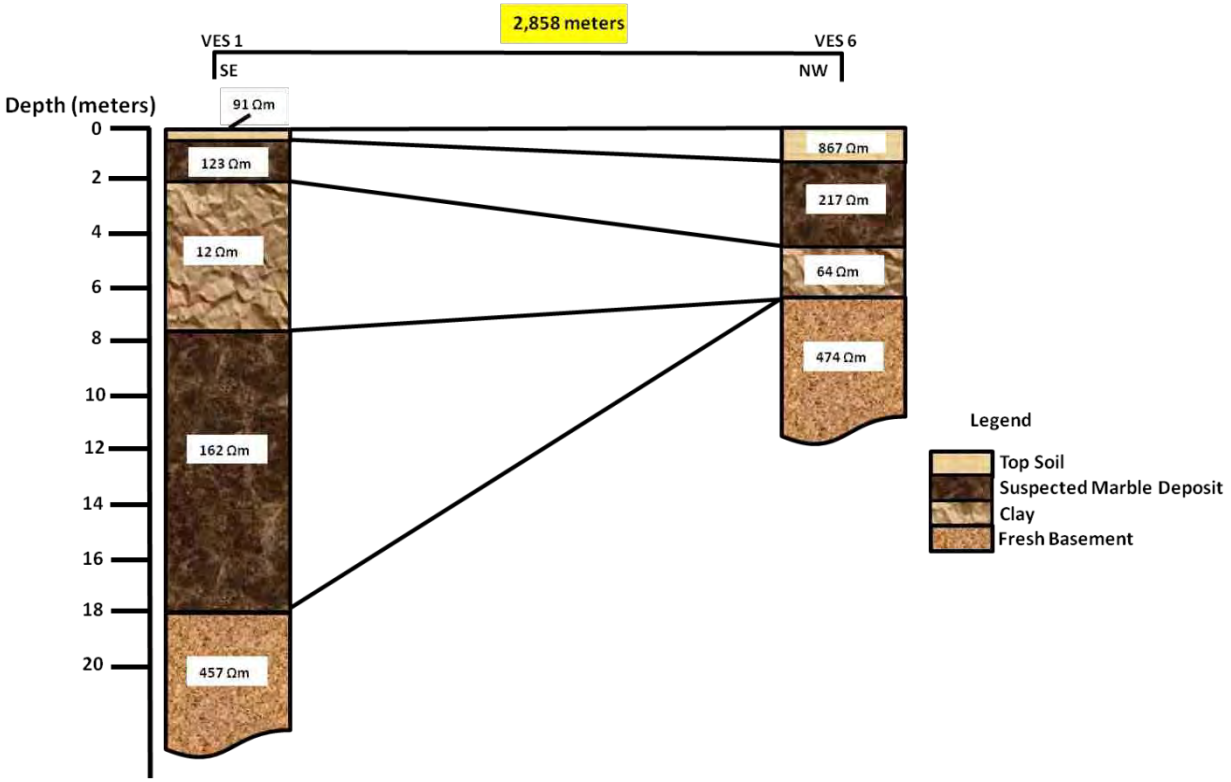


Figure 18: Correlation Panel for Columnar Sections for VES 1 and VES 6

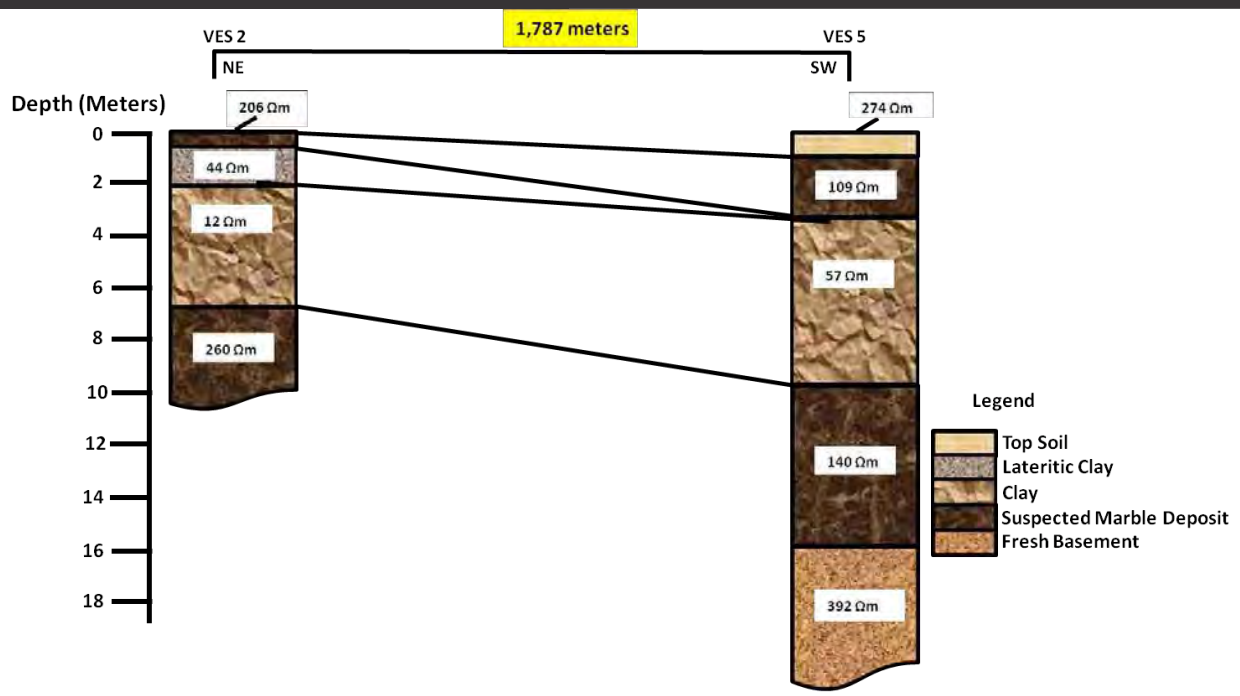


Figure 19: Correlation Panel for Columnar Sections for VES 2 and VES 5

value. The top soil has resistivity values in the range of 206–274 Ωm and thickness values in the range of 0.7–1 m. This layer is underlain by Lateritic Clay with resistivity value of 44 Ωm and thickness value of 1.3 m at VES 2; suspected marble deposit with resistivity value of 109 Ωm and thickness of 2.3 m at VES 5. These layers are further underlain by Clay with resistivity values in the range of 12–57 Ωm and thickness values in the range of 5.2–6.4 m. Another suspected marble deposit underlies the clay layer with resistivity values in the range of 140–260 Ωm, with indeterminate thickness at VES 2 and thickness value of 6.2 m. The last layer with resistivity value of 392 Ωm with infinite thickness is the fresh basement (Figure 19).

The distance between VES 2 and VES 5 is 1,787 m. There is a noticeable absence of Marble deposit at the top soil of VES 5. However, other geoelectric/geologic layers for both columnar sections correlate well with each other with varying thicknesses. Suspected marble deposit is also observed at depth of approximately 7.7 m at VES 2 and VEs 5. The depth to the top of the Marble at VES 2 is observed to be shallower than VES 4, with an observable dip towards the southwestern part of the study area at VES 5. The lateral extent of the Marble deposit is approximately 1,787 m based on the distance between the two VES points (Figure 19).

Figure 20 shows the correlation panel connecting columnar sections of VES 2 and VES 6. The columnar sections obtained for VES 2 and VES 6 identified three to four geoelectric/geologic subsurface layers which include the top soil, Lateritic Clay, Clay, suspected Marble deposit and fresh basement with relatively high resistivity value. The top soil has resistivity values in the

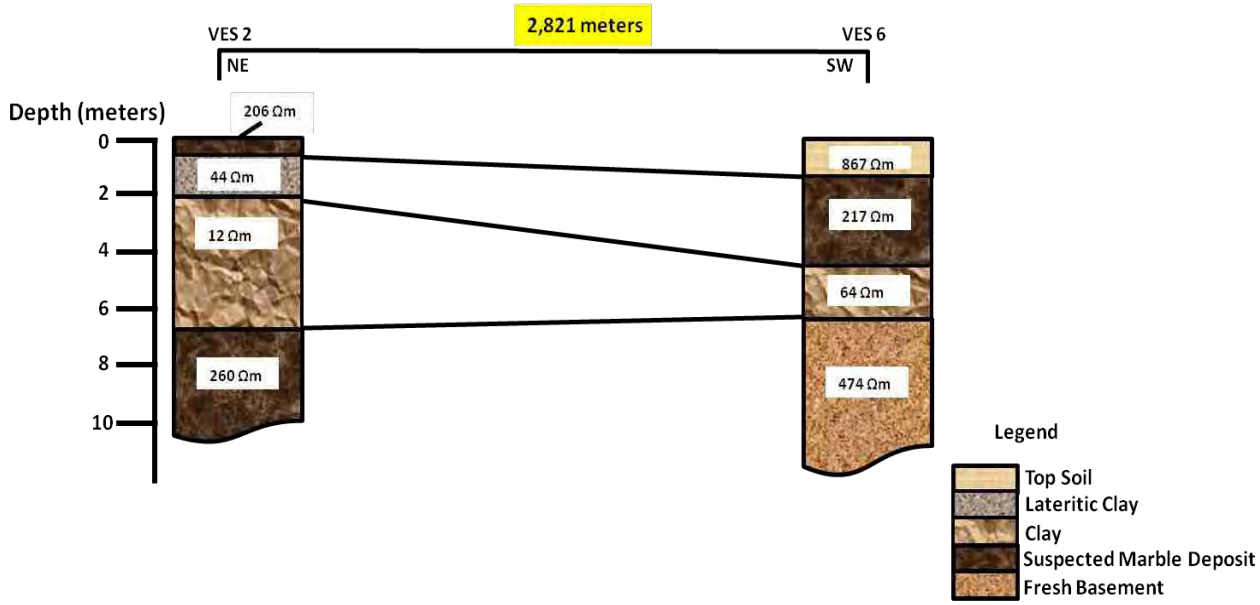


Figure 20: Correlation Panel for Columnar Sections for VES 2 and VES 6

range of 206–867 Ωm with thickness values in the range of 0.7–1.3 m. This layer is underlain by Lateritic Clay with resistivity value of 44 Ωm and thickness value of 1.3 at VES 2, while a suspected marble deposit with resistivity value of 217 Ωm and thickness value of 3.2 occur at VES 6. This layer is further underlain by Clay with resistivity values in the range of 12–64 Ωm and thickness values in the range of 1.8–5.2 m. The last layer is underlain by suspected marble deposit with resistivity value of 260 Ωm at VES 2; and fresh basement with resistivity value of 474 Ωm at VES 6 with infinite thicknesses (Figure 20).

The distance between VES 2 and VES 6 is 2,821 m. There are visible outcrops of marble at VES 2 which guided the interpretation of the geoelectric and geologic layers. On the other hand, there is a noticeable absence of Marble deposit at the top soil of VES 6. The depth to the top of the Marble at VES 2 is observed to be relatively shallower than VES 4, with an observable dip towards the southwestern part of the study area at VES 6. The lateral extent of the Marble deposit is approximately 2,821 m based on the distance between the two VES points (Figure 20).

Figure 21 shows the the correlation panel connecting columnar sections of VES 3 and VES 6. The columnar sections obtained for VES 3 and VES 6 identified four geoelectric/geologic subsurface layers which include the top soil, Clay, suspected marble deposit and fresh basement with relatively high resistivity value. The top soil has resistivity values in the range of 475–867 Ωm and thickness values in the range of 1–1.3 m. This layer is underlain by suspected marble deposit with resistivity values in the range of 144–217 Ωm and thickness values in the range of 1.5–3.2 m; Clay with resistivity values in the range of 18–64 Ωm and thickness values in the range of 1.8–5.2 m; another suspected marble deposit with resistivity value of 148 Ωm and thickness value of 3.7 m at VES 3. The last layer with resistivity values in the range of 474–1092 Ωm with infinite thickness is the fresh basement (Figure 21).

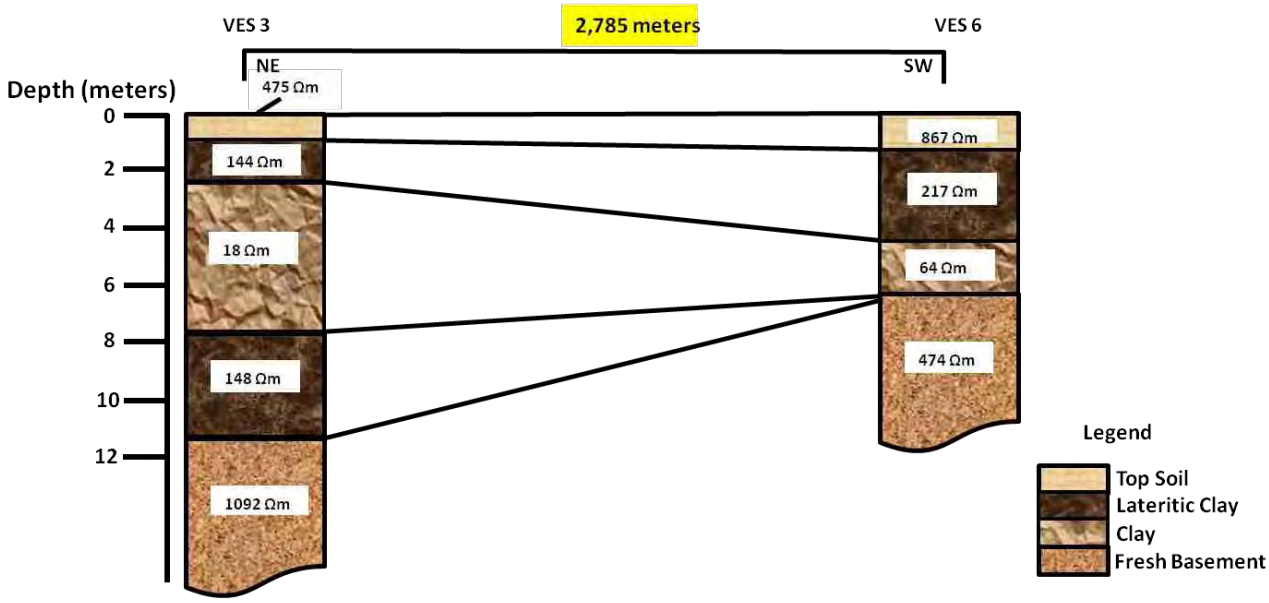


Figure 21: Correlation Panel for Columnar Sections for VES 3 and VES 6

The distance between VES 3 and VES 6 is 2,785 m. The underlying geoelectric/geologic layers for both columnar sections correlate well with each other, howbeit with varying thicknesses especially for the Clay. The suspected marble deposit is observed to be truncated by clay layer at VES 3 with a noticeable absence at depth on VES 6. He suspected marble deposit is observed to thicken towards VES 6, with an observable extension at VES 3. The lateral extent of the Marble deposit is approximately 2,785 m based on the distance between the two VES points (Figure 21).

Figure 22 shows the correlation panel connecting columnar sections of VES 4 and VES 5. The columnar sections obtained for VES 4 and VES 5 identified four geoelectric/geologic subsurface layers which include the top soil, suspected marble deposit, Clay and fresh basement with relatively high resistivity value. The top soil has resistivity values in the range of 274–578 Ωm with thickness values in the range of 0.8–1 m. This layer is underlain by suspected marble deposit with resistivity values in the range of 109–112 Ωm and thickness values in the range of 1.2–2.3 m; Clay with resistivity values in the range of 34–57 Ωm and thickness values in the range of 6–6.4 m. This is further underlain by suspected marble deposit with resistivity values in the range of 140–184 Ωm and thickness values in the range of 6.2–7 m. The last layer with resistivity values in the range of 392–1241 Ωm with infinite thickness is the fresh basement (Figure 22).

The distance between VES 4 and VES 5 is 1,909 m. The underlying geoelectric/geologic layers for both columnar sections correlate well with each other, howbeit with varying thicknesses especially for the Clay layer. The depth to the top of the Marble at VES 4 is observed to be relatively shallower than VES 5, with an observable dip towards the southwestern part of the study area at VES 5. The correlation panel further showed that

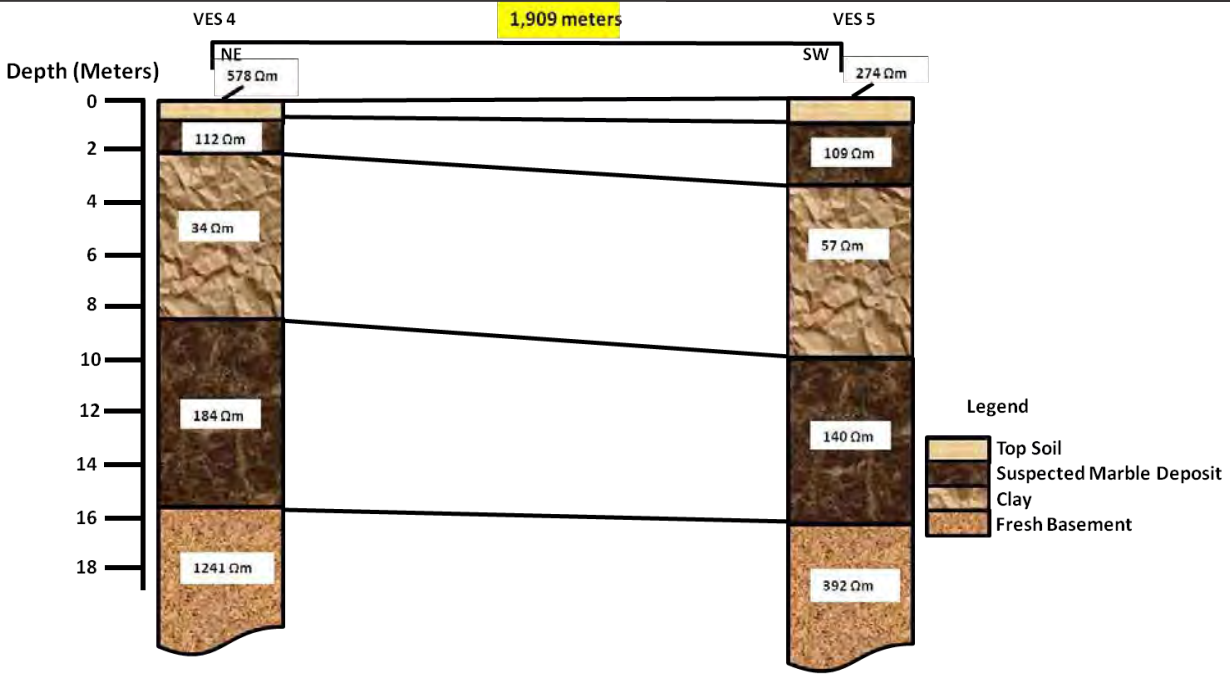


Figure 22: Correlation Panel for Columnar Sections for VES 4 and VES 5

the suspected marble deposit is truncated by clay layer at a depth of about 2.3 m, having thickness of approximately 6 m. The lateral extent of the Marble deposit is approximately 1,909 m based on the distance between the two VES points (Figure 22).

Figure 23 shows the correlation panel connecting columnar sections of VES 4 and VES 6. The columnar sections obtained for VES 4 and VES 6 identified four geoelectric/geologic subsurface layers which include the top soil, suspected marble deposit, Clay and fresh basement with relatively high resistivity value. The top soil has resistivity values in the range of 578–867 Ωm and thickness values in the range of 0.8–1.3 m. This layer is underlain by suspected marble deposit with resistivity values in the range of 112–217 Ωm and thickness values in the range of 1.2–3.2 m; Clay with resistivity values in the range of 34–64 Ωm and thickness values in the range of 1.8–6 m. Another suspected marble deposit with resistivity value of 184 Ωm and thickness of 7 m is observed at VES 4. The last layer with resistivity values in the range of 474–1241 Ωm constitutes the fresh basement (Figure 23).

The underlying geoelectric/geologic layers for both columnar sections correlate well with each other, howbeit with varying thicknesses especially for the Lateritic Clay and Clay. The suspected marble deposit at the near surface is observed to thicken in the northwestern direction around VES 6. The suspected marble deposit extends to a depth of approximately 6.3 m where it is truncated by a clay unit having thickness of about 6 m. However, the suspected marble deposit is observed to be absent at depth at VES 6. The lateral extent of the Marble deposit is approximately 2,983 m based on the distance between the two VES points (Figure 23).

Figure 24 shows the correlation panel connecting columnar sections of VES 5 and VES 6. The

columnar sections obtained for VES 5 and VES 6 identified four geoelectric/geologic subsurface layers which include the top soil, suspected marble deposit, Clay and fresh basement with relatively high resistivity value. The top soil has resistivity values in the range of 274–867 Ωm and thickness values in the range of 1–1.3 m. This layer is underlain by suspected marble deposit with resistivity values in the range of 109–217 Ωm and thickness values in the range of 2.3–3.2 m; Clay with resistivity values in the range of 57–64 Ωm and thickness values in the range of 1.8–6.4 m. Another suspected marble deposit with resistivity value of 140 Ωm and thickness of 6.2 m is observed at VES 5. The last layer with resistivity values in the range of 392–474 Ωm with infinite thickness constitutes the fresh basement in the study area (Figure 24).

The distance between VES 5 and VES 6 is 1,594 m. The underlying geoelectric/geologic layers for both columnar sections correlate well with each other, howbeit with varying thicknesses especially for the Clay unit. The suspected marble deposit is observed to be near surface, but with a continuous occurrence of marble at VES 5 where it is truncated by a clay unit of 6. 4 m thickness. However, there is a noticeable absence of the suspected marble deposit at depth at VES 6. The marble deposit is observed to thicken towards the northwestern part of the study area around VES 6. The lateral extent of the Marble deposit is approximately 1,594 m based on the distance between the two VES points (Figure 24).

Conclusion

This study involves the integration of ASTER and geoelectric resistivity datasets in the mapping of Marble deposits, in Ogale area, Igarra Schist belt,

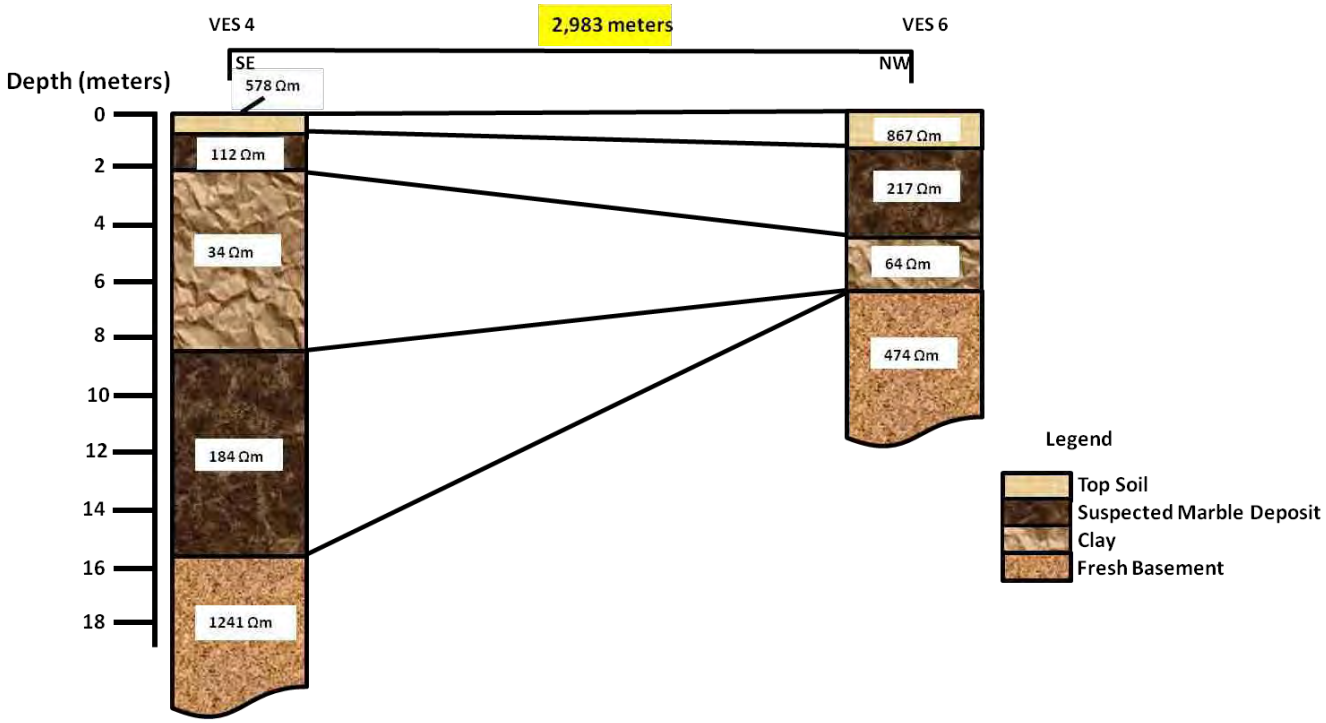


Figure 23: Correlation Panel for Columnar Sections for VES 4 and VES 6

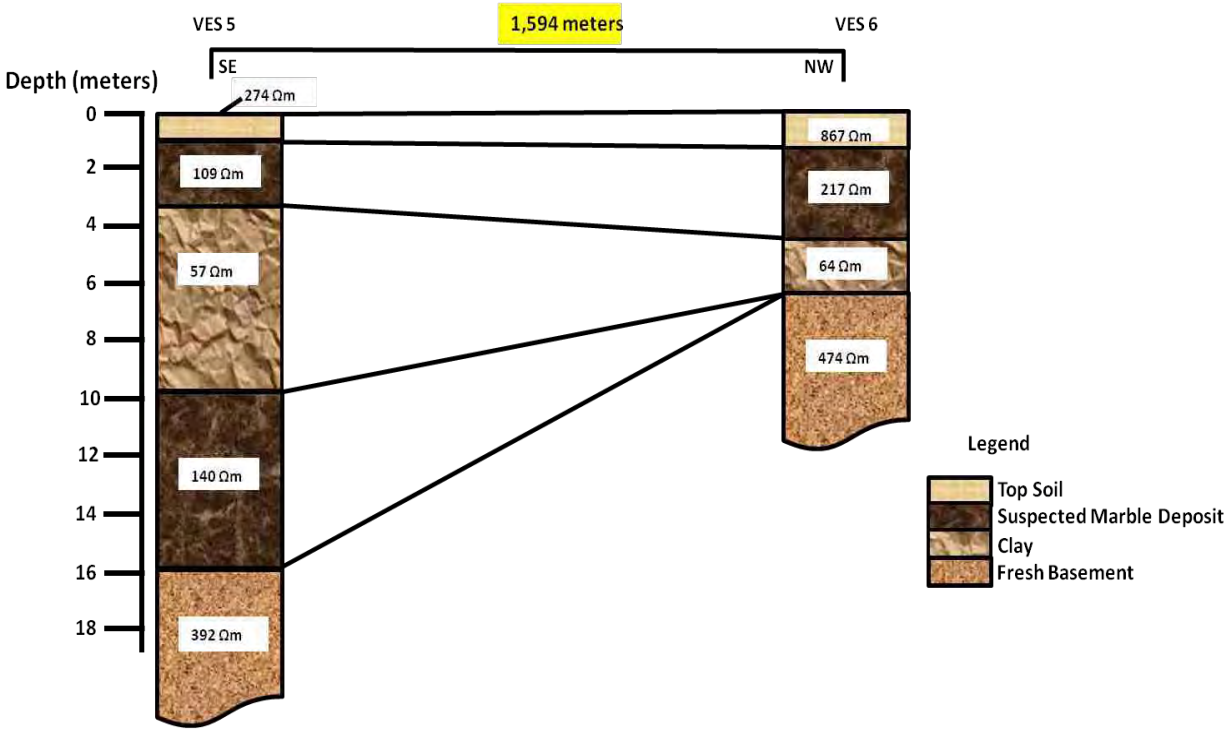


Figure 24: Correlation Panel for Columnar Sections for VES 5 and VES 6

Kogi State, Nigeria.

Zones of marble mineralization were mapped on the ASTER dataset by combining the bands in form of RGB composite maps of the bands and decorrelation stretch of the bands to highlight areas of marble mineralization due to presence of carbonate materials in the subsurface. Band combinations of (3, 9, 14), (4, 9, 8), (4, 6, 8), (14, 8, 6), (14, 8, 4), (8, 4, 3), (6, 8, 9) and (4, 8, 9) were applied for the effective mapping of marble mineralization.

The results of the processed imageries indicate that marble mineralization is found exclusively in the western parts of the study area. This also extends as few patches in the southern and eastern parts of the study area. Geoelectric soundings were subsequently carried out in the delineated prospective zones. Results from the VES showed that the area is underlain by three to five geoelectric/geologic layers comprising the top soil, lateritic layer, clay unit, weathered layer and the Marble hosted basement.

From the results of the VES, eight correlation panels were generated for the six VES points. The correlation panel results confirmed analysis of the ASTER imagery that marble mineralization is dominant in the western part of the study area. The results also showed that the suspected marble deposit in the study area occurs to an average depth of 10 m. This indicates that marble mineralization is occurring in the near subsurface.

The study therefore concludes that ASTER and geoelectric sounding datasets are effective in the mapping of marble deposits. Furthermore, the study revealed that marble mineralization occurs in the study area, and the methods used in this study can be adopted for marble exploration in similar geologic setting like the study area.

REFERENCES

Abatan, S. O., Odukoya, A. A., Ehimiyen, U. A. & Bankole, B.O. (1993). Limestone and Shale investigation for cement manufacture at Somo, near Shagamu, Ogun State. Geological Survey of Nigeria, Abeokuta, Report, 110p.

Aina, A.O. & Olorunfemi, M.O. (1996). Comparative fild results for electrical resistivity, magnetic, gravity and VLF methods over a marble lens. *Exploration Geophysics, Vol.* 27, pp. 217-222.

Ajigo, I.O., Ademeso, O.A. & Odeyemi, I.B. (2020). Integrated geological and geophysical data as an aid to surface geological mapping and mineral exploration of the Ibillo–Okene area, Southwest Nigeria. An unpublished Ph.D Thesis, Federal University of Technology, Akure, Nigeria, 185p.

Akinlalu, A.A., Afolabi, D.O. & Sanusi, S.O. (2024). Knowledge–Driven Fuzzy AHP model for orogenic gold prospecting in a typical schist belt environment: A mineral system approach. *Earth Systems and Environment*. pp. 1–43. https://doi.org/10.1007/s41748-024-00382-4.

Baldridge, A.M., Hook, S.J., Grove, C.I. & Rivera, G. (2009). The ASTER spectral library version 2.0. Remote Sens. Environ., Vol. 11 (3), pp. 711–715.

Clark, R.N. (1999). Spectroscopy of rock and minerals and principles of spectroscopy. In: Rencz, A.N. (Ed.), Remote Sensing for the Earth Sciences: Manual of Remote Sensing, Vol. 3, John Wiley & Sons, New York, pp. 3–58.

Federal Ministry of Information and Culture (FMIC), Abuja (1999). Nigeria Hand Book. pp.5–8.

Fatoye, F.B. & Gideon, Y.B. (2013). Geology and occurrences of limestone and marble in Nigeria. *Journal of Natural Sciences Research*, Vol. 3(11), pp. 60-65.

Gaffey, S.J. (1986). Spectral reflectance of carbonate minerals in the visible and near infrared (0.35–2.55 microns): calcite, aragonite, and dolomite. Am. *Mineral*., Vol. 71, pp. 151–162.

Gillespie, A. R., Matsunaga, T., Rokugawa, S., & Hook, S. J. (1998). Temperature and emissivity separation from Advanced Spaceborne Thermal Emission and Reflection Radiometer (ASTER) images. *IEEE Trans Geosci Remote Sens, Vol.* 36, pp. 1113–1126.

Iwasaki A. & Tonooka H. (2005). Validation of a crosstalk correction algorithm for ASTER/SWIR. *IEEE Trans Geosci Remote Sens., Vol.*43(12), pp. 2747–2751. https://doi.org/10.1109/TGRS.2005.855066.

Keller, G.V., & Frischnecht, F.C. (1966.). Electrical Methods in Geophysical Prospecting. Pergamon Press: Oxford, UK. 523pp.

Klynveld Peat Marwick Goerdeler, (KPMG) (2017). Third edition of Nigeria Mining Sector Brief. 32pp.

Koefeod, O. (1979). Geosounding Principles, 1. Resistivity Sounding Measurements. Elsevier Scientific Publishing Comp.: Amsterdam, The Netherlands. 275pp.

Madani, A. (2014). Assessment and evaluation of band ratios, Brovey and HSV techniques for lithologic discrimination and mapping using Landsat ETM+ and SPOT-5 data. *International Journal of Geosciences,* Vol. 5, pp. 5-11.

Mars, J. C., & Rowan, L. C. (2006). Regional mapping of phyllic-and argillic-altered rocks in the Zagros magmatic arc, Iran, using Advanced Spaceborne Thermal Emission and Reflection Radiometer (ASTER) data and logical operator algorithms. *Geosphere*, Vol. *2*(3), pp. 161-186.

Mars, J.C. & Rowan, L.C. (2011). ASTER spectral analysis and lithologic mapping of the Khanneshin carbonatite volcano, Afghanistan. *Geosphere*, Vol.*7*, pp. 276–289.

Ninomiya, Y., Fu, B. & Cudahy, T.J. (2005). Detecting lithology with advanced spaceborne thermal emission and reflection radiometer (ASTER) multispectral thermal infrared "radiance-atsensor" data. *Remote Sens. Environ., Vol.* 99, pp. 127–139.

Obaje, N.G. (2009). Geology and mineral resources of Nigeria. Springer, London, Dordrecht. 222p.

Odeyemi, I. B. (1988): *Lithostratigraphy and structural relationships of the Upper Precambrian Metasediments in Igarra area, southwestern Nigeria*. In: Oluyide, P. O., W. C. Mbonu, A. E. Ogezi, I. G. Egbuniwe, A. C. Ajibade, and A. C. Umeji. (editors), Precambrian geology of Nigeria. Published by Nigerian Geological Survey Agency. Pp.111 – 125.

Odeyemi, I. B. (1990). The petrology of a Pan-African pluton in Igarra, southwestern Nigeria. *Nigerian Journal of Science., Vol.* 28 (2), pp. 181-193.

Odeyemi, I.B. (1993). A Comparative study of remote sensing images of the structure of Okemesi Fold Belt, Nigeria. *ITC J., Vol. 1, pp.* 77–81.

Odeyemi, I. B., Olorunniwo, M. A. & Folami, S. I. (1997a). Late-proterozoic metaconglomerates in the schist belt of Nigeria: origin and techonostratigraphic significance revisited. *Journal of Technoscience.*, Vol.1(3), pp. 48-55.

Odeyemi, I.B., Oloruniwo, M.A. & Folami, S.L. (1997b). Geological and geophysical characteristics of Ikpeshi marble deposit, Igarra area, southwestern Nigeria. *Journal of Mining and Geology, Vol.* 33, pp. 63-79.

Olade, M. A. (2019). Geological re-evaluation of Nigeria's iron ore deposits as raw materials`for a viable iron and steel industry. *Achievers J Scient Res*, Vol. *2*(1), pp. 1-22.

Onimisi, M., Abaa, S.I,, Obaje, N.G. & Sule, V.I. (2015) A Preliminary Estimate of the Reserve of the Marble Deposit in Itobe Area, Central Nigeria. *Journal of Geology & Geophysics* Vol. 4, pp 216. https://doi:10.4172/2381-8719.1000216

Orellana, E., & Mooney, H. M. (1966). Master Tables and Curves for Vertical Electrical Sounding over Layered Structures. Inteciencis, Madrib. Vol. 34.

Ozegin, K.O. (2019). Exploration for marble deposit in parts of Okpella, south-southern Nigeria. *Journal of Geography, Environment and Earth Science*

International., Vol. 22 (3), pp.1–7.

Raw Materials Research and Development Council (RMRDC), Abuja (2001). Technical Brief on Minerals in Nigeria–Limestone/Marble. pp. 1–17.

Rajendran, S., Hersi, O.S., Al-Harthy, A.R., Al-Wardi, M., Ali El-Ghali, M. & Al-Abri, A.H. (2011a). Capability of advanced spaceborne thermal emission and reflection radiometer (ASTER) on discrimination of carbonates and associated rocks and mineral identification of Eastern Mountain region (Saih Hatat Window) of Sultanate of Oman. *Carbonates Evaporites*., Vol. 26, pp. 351– 364.

Rajendran, S., Thirunavukkarasu, A., Balamurugan, G. & Shankar, K. (2011b). Discrimination of iron ore deposits of granulite terrain of Southern Peninsular India using ASTER data. *J. Asian Earth Sci., Vol.* 41, pp. 99–106.

Rajendran, S., Al-Khirbash, S., Pracejus, B., Nasir, S., Al-Abri, A.H., Kusky, T.M. & Ghulam, A. (2012). ASTER detection of chromite bearing mineralized zones in semail ophiolite massifs of the northern Oman mountain: exploration strategy. *Ore Geol. Rev*., Vol. 44, pp. 121–135.

Rajendran, S. & Nasir, S. (2013a). ASTER spectral analysis of ultramafic lamprophyres (carbonatites and aillikites) within the Batain nappe, northeastern margin of Oman – a proposal developed for spectral absorption. *Int. J. Remote Sens.,* Vol. 34 (8), pp. 2763–2795.

Rajendran, S. & Nasir, S. (2013b). ASTER mapping of limestone formations and study of caves, springs and depressions in parts of Sultanate of Oman. *Environ. Earth Sci.,* Vol. 71(1), pp. 133-146. http://dx.doi.org/10.1007/s12665-013-2419-7.

Rowan, L.C., Kingston, M.J., Crowley, & J.K. (1986). Spectral reflectance of carbonatite and related alkalic igneous rocks from four North American localities. *Econ. Geol.* Vol. 81, pp. 857–871.

Thome, K., Palluconi, F., Takashima, T. & Masuda, K. (1998). Atmospheric correction of ASTER. IEEE Trans Geosci Remote Sens, Vol. 36 (4), pp. 1119–1211.

Vander-Velpen, B.P.A. (1989). RESIST Version 1.0. M.Sc. Research Project. ITC: Delft Netherlands.

Zohdy, A.A.R. (1965). The Auxiliary Point Method of Electrical Sounding Interpretation and its Relationship to Dar Zorrouk Parameters". Geophysics, Vol. 30, pp. 644-650.